Check for updates

Exploration

REVIEW OPEN ACCESS

Enhancing Stability in Next-Generation Photoelectrodes Such as Organic Semiconductor and Halide Perovskite-Based Photoelectrodes for Various Applications: Recent Advanced Passivation and Encapsulation Methods

Yejoon Kim[1] | Enok Lee[1] | Sanghan Lee[1,2]

[1]Department of Materials Science and Engineering, Gwangju Institute of Science and Technology, Gwangju, Republic of Korea | [2]Research Institute for Solar and Sustainable Energies, Gwangju Institute of Science and Technology, Gwangju, Republic of Korea

Correspondence: Sanghan Lee (sanghan@gist.ac.kr)

Received: 24 June 2024 | **Revised:** 28 August 2024 | **Accepted:** 8 January 2025

Keywords: bias-free system | encapsulation | halide perovskite | organic semiconductor | passivation | photoelectrochemical

ABSTRACT

This review explores advancements in passivation and encapsulation methods for organic semiconductor (OS) and halide perovskite (HP)-based photoelectrodes, aimed at enhancing stability in photoelectrochemical (PEC) systems. The integration of OS and HP materials in PEC devices offers high photovoltage and impressive current densities, promising efficient solar-to-fuel conversion and pollutant upcycling. However, these materials face significant intrinsic and extrinsic degradation under PEC conditions. We discuss various passivation strategies to mitigate photochemical reactions and defect-related degradation, as well as advanced encapsulation techniques to prevent electrolyte-induced corrosion. The review highlights the latest research on enhancing the operational stability and performance of OS and HP-based photoelectrodes, emphasizing their potential in sustainable energy applications and environmental remediation. Future research directions include optimizing material design, exploring new passivation and encapsulation technologies, and scaling up for practical applications. This comprehensive review underscores the critical role of material innovation in advancing PEC technology for a sustainable future.

1 | Introduction

As global energy demand continues to rise, the pursuit of sustainable energy solutions has become increasingly urgent, leading to active exploration of innovative technologies that leverage solar power for efficient energy conversion [1–3]. Among these technologies, photoelectrochemical (PEC) systems, which integrate photovoltaic (PV) and electrochemical (EC) cells into a single device using photoelectrodes, show significant potential for directly converting solar energy into storable fuels without intermediate steps [4–6]. Consequently, the photoelectric and electrochemical properties of the photoelectrodes directly impact the overall system performance. Notably, the photoelectric properties, represented by the open-circuit voltage and short-circuit current density of the photoelectrodes, are the primary factors in evaluating the performance of PEC systems. However, conventional PEC systems based on silicon [7, 8], III–V semiconductors [9, 10], and metal oxide photoelectrodes [11–13] have demonstrated unsatisfactory photoelectric properties, often relying on external bias to drive redox reactions. This dependency introduces issues related to energy efficiency, system complexity, and cost-effectiveness. To address these challenges

Yejoon Kim and Enok Lee contributed equally to this work.

This is an open access article under the terms of the Creative Commons Attribution License, which permits use, distribution and reproduction in any medium, provided the original work is properly cited.

© 2026 The Author(s). *Exploration* published by Henan University and John Wiley & Sons Australia, Ltd.

and create an ideal PEC system that operates without external voltage, efforts have been made to convert next-generation solar cells with superior photoelectric properties into photoelectrodes [14]. Specifically, organic semiconductor (OS) and halide perovskite (HP)-based photoelectrodes have garnered significant attention due to their potential for large-scale commercialization. Both materials exhibit excellent light absorption across a broad spectrum and can be tuned to achieve desirable properties for PEC systems [15–17]. Additionally, solution printing processes based on organic solvents make them suitable for low-cost, large-area device fabrication [18, 19]. OS and HP-based photoelectrodes have demonstrated remarkable photoelectric properties, including open-circuit voltages exceeding 1.0 V and current densities in the tens of mA cm^{-2}, along with unparalleled solar conversion efficiencies compared to other single light-absorbing layer materials [20–24].

However, early OS and HP-based photoelectrodes exhibited extremely poor operational stability, completely failing within hours, compared to the hundreds of hours of operational time demonstrated by conventional photoelectrodes [25–28]. This stability issue arises from the harsh operating conditions of PEC systems, which differ significantly from those of PV systems. In PEC systems, the external circuit between the two electrodes is composed of an electrolyte, which relies on ion conduction rather than the rapid electron transfer that occurs in traditional metal wires [29]. For ion conduction to occur, electrochemical reactions must take place, introducing significant resistance to the overall circuit and causing charge accumulation within the device. Defects in the materials comprising the photoelectrodes serve as recombination sites for the accumulated charges, initiating degradation [30, 31]. Consequently, the stability of OS and HP-based photoelectrodes is much lower than that of PV devices with the same structure, with degradation occurring more frequently and extensively. Therefore, the development of highly stable OS and HP PV devices is essential before converting them into photoelectrodes. This requires a deep understanding of the materials and the introduction of meticulous passivation techniques.

Moreover, photoelectrodes operating in electrolytes face inevitable corrosion or decomposition in aqueous electrolytes, to which OS and HP-based photoelectrodes are particularly vulnerable. While conventional photoelectrodes also experience electrochemical corrosion in aqueous electrolytes, they tend to remain relatively stable in the absence of external voltage due to their strong covalent bonds. In contrast, OS and HP-based photoelectrodes, typically fabricated through solution coating processes with organic solvents, cannot withstand such conditions and decompose in the electrolyte, leading to immediate device failure [32, 33]. Therefore, when converting OS and HP PV devices into photoelectrodes, it is very important to apply encapsulation methods that can prevent the infiltration of aqueous electrolytes. These encapsulation methods should be designed to minimize internal resistance and performance degradation (Figure 1).

In this review, we explore the structures of solar cells and photoelectrodes with single OS and HP light-absorbing layers, investigate degradation mechanisms that may occur in each structure, and discuss suitable passivation methods to achieve high operational stability in electrolyte environments. Additionally, we summarize various encapsulation methods to block the penetration of aqueous electrolytes, assessing the advantages and disadvantages of each approach. Finally, we highlight various PEC systems, such as water splitting and CO_2 reduction, utilizing OS and HP-based photoelectrodes. We expect that focusing on the design and development of OS and HP-based photoelectrodes will lead to significant advancements in the environmentally friendly PEC field.

2 | Structure of OS and HP-Based Photoelectrodes

The basic structure of OS and HP-based photoelectrodes is the same as that of solar cells. It follows a sandwich structure where the charge transport layers and electrodes are sequentially positioned around the light-absorbing layer [34, 35]. This structure is carefully crafted considering the overall energy band diagram, promoting effective separation of electrons and holes, and their conversion into current and power [36, 37]. In this chapter, to ensure a smooth understanding of the overall review and provide fundamental insights into device design, we will explore the principles and representative materials used in the structure of OS and HP-based devices.

2.1 | Light-Absorbing Layer

The light-absorbing layer, also known as the 'active layer,' is the most distinctive structure of OS and HP-based photoelectrodes. It absorbs sunlight to generate charge carriers (electrons and holes), which then move along the electric field to form a current [38, 39]. The active layer plays a crucial role in both types of photoelectrodes, absorbing sunlight and generating electrical energy, each comprising unique materials and structures. Commonly used materials are summarized in Table 1. Additionally, the efficiency of the active layer is a critical factor determining the overall performance of solar cells [40, 41].

In OS-based active layers, donor and acceptor materials are typically composed of polymers and fullerene derivatives [69, 70]. The donor donates electrons, while the acceptor receives electrons. The bulk-heterojunction structure, where donor and acceptor materials are mixed on a nanometer scale, enhances light absorption and charge separation efficiency [69, 71]. When sunlight is absorbed by the donor material, excitons (electron–hole pairs) are generated. These excitons are separated into electrons and holes at the donor–-acceptor interface [72]. The separated electrons and holes then move to the electrodes through the acceptor and donor materials, respectively, forming a current through the external circuit.

The active layer in HP-based photoelectrodes consists of materials with a halide perovskite structure of ABX_3 [73]. Here, A-site represents an organic/inorganic cation (e.g., methylammonium (MA), formamidinium (FA), Cs^+, Rb^+), B-site represents a metal cation (e.g., Pb^{2+}, Sn^{2+}), and X-site represents a halide anion (e.g., I^-, Br^-, Cl^-). The formation of the ABX_3 crystal structure is determined by the tolerance factor, t, which is defined by the formula below;

$$t = (rA + rX)/[\sqrt{2}(rB + rX)] \quad (1)$$

27662098, 2026, 1, Downloaded from https://onlinelibrary.wiley.com/doi/10.1002/EXP.20240020 by CochraneChina, Wiley Online Library on [08/06/2026]. See the Terms and Conditions (https://onlinelibrary.wiley.com/terms-and-conditions) on Wiley Online Library for rules of use; OA articles are governed by the applicable Creative Commons License

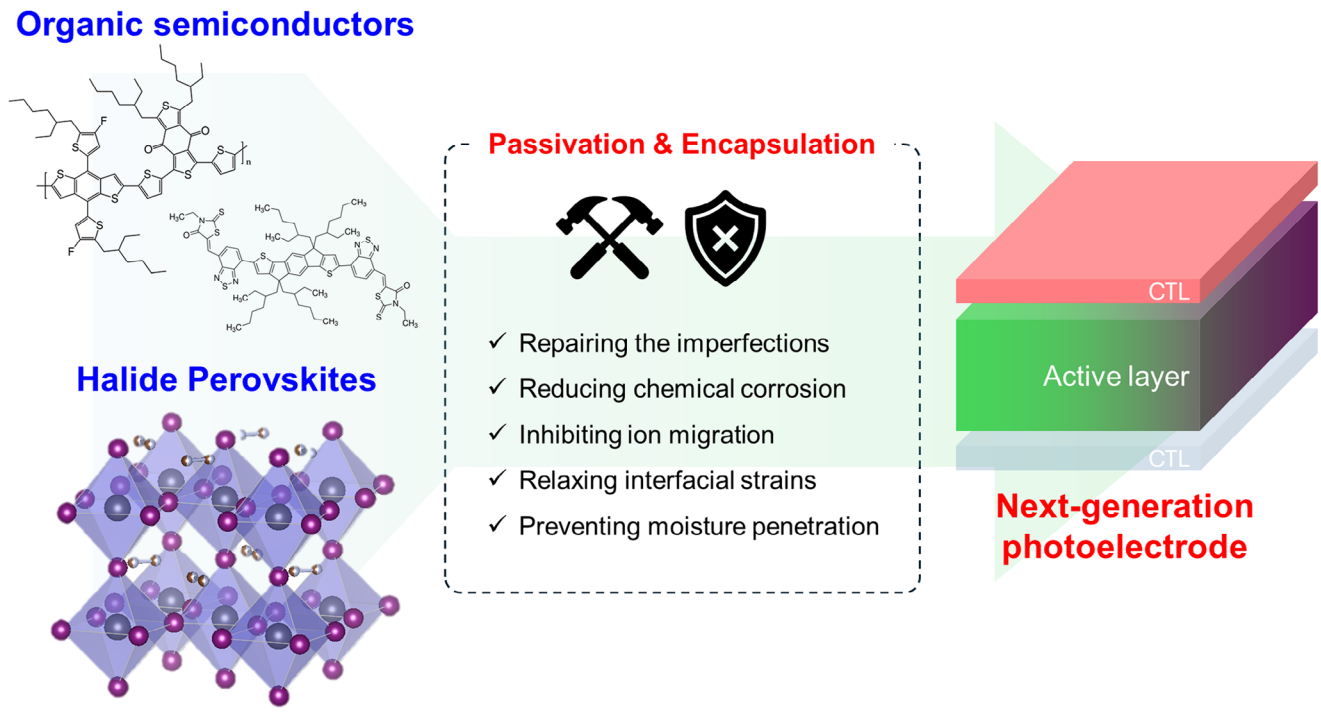


FIGURE 1 | Strategies for OS and HP passivation and encapsulation to fabricate next-generation photoelectrodes.

where *r*A and *r*B are the ionic radii of the A-site and B-site cations, respectively, and *r*X is the ionic radius of the X-site anion [74]. It is generally reported that perovskites form in the range $0.8 \leq t \leq 1$. Uniquely, the bandgap of the HP-based active layers can be tuned freely by changing or mixing the halide X-site [75].

2.2 | Charge Transport Layer

The charge transport layer (CTL) is located above and below the active layer, efficiently extracting charge carriers (electrons and holes) and transporting them to the respective electrodes. This is essential for generating current and enhancing power conversion efficiency. CTL is divided into the electron transport layer and the hole transport layer, each promoting the movement of electrons and holes, respectively.

- Electron transport layer (ETL): ETL collects electrons generated in the active layer and transfers them to the cathode. ETL must have high electron mobility and suitable energy levels, minimizing electron recombination to enhance electron transport efficiency [76–78]. It is typically composed of n-type semiconductor materials.
- Hole transport layer (HTL): HTL collects holes generated in the active layer and transfers them to the anode. HTL must have high hole mobility and suitable energy levels, minimizing hole recombination to enhance hole transport efficiency [79]. It is typically composed of p-type semiconductor materials.

The CTL provides pathways for the movement of electrons and holes, minimizing recombination and optimizing charge transport to the electrodes, thereby increasing the efficiency of solar cells. Additionally, the CTL adjusts the energy barriers between the active layer and the electrodes to facilitate the extraction of electrons and holes. The materials used for the CTL should be appropriately selected based on the energy band structure of the active layer [78–80]. Popular materials for ETL and HTL are summarized in Table 2.

2.3 | Electrodes

Electrodes, anodes and cathodes, play a crucial role in collecting electrons and holes and transferring them to the external circuit. To allow the active layer to absorb light, one electrode must be a transparent electrode with high transmittance [95]. Typically, transparent conductive materials with high optical transparency and low resistance are used. Representative materials include indium tin oxide (ITO) and fluorine-doped tin oxide (FTO).

For the anode, materials with a high work function are necessary to facilitate hole collection. These materials align well with the energy levels of the HTL, aiding in the effective extraction of holes. Examples include gold (Au) [96], platinum (Pt) [97], and nickel (Ni) [97]. The cathode, which collects electrons and transfers them to the external circuit, utilizes metals with a low work function to optimize electron collection. These materials match the energy levels of the ETL, promoting efficient electron extraction and transport. Common examples are aluminum (Al) [98], silver (Ag) [99], and calcium (Ca) [100]. High work function materials facilitate hole extraction in the HTL, while low work function materials ease electron extraction in the ETL, minimizing energy barriers, and optimizing charge transport pathways.

27662098, 2026, 1, Downloaded from https://onlinelibrary.wiley.com/doi/10.1002/EXP.20240020 by CochraneChina, Wiley Online Library on [08/06/2026]. See the Terms and Conditions (https://onlinelibrary.wiley.com/terms-and-conditions) on Wiley Online Library for rules of use; OA articles are governed by the applicable Creative Commons License

TABLE 1 | Summarization of the OS and HP-based active layer materials.

Organic semiconductor-based active layer	
Type	**Materials**
Polymer donors	P3HT[a], [42] PTB7-Th[b] [43], PCDTBT[c] [44], PBDB-T-2F[d] [45], PffBT4T[e] [46], PBDB-T[f] [47], etc.
Small molecule donors	DPP-DTT[g] [48], BDT[h] [49], IT-4F[i] [50], SM1[j] [51], SM2[k] [51], etc.
Fullerene acceptors	PCBM[l] [52], $PC_{71}BM$[m] [53], other C_{60}-derivatives [54], etc.
Non-fullerene acceptors	ITIC[n] [47], BTP-4F[o] [55], IDTBR[p] [42], IDIC[q] [56], ITIC-M[r] [57], IEICO-4F[s] [58], FBR[t] [59], etc.
Halide perovskite active layer	
Type	**Materials**
Halide perovskites	$MAPbI_3$-Br_3-Cl_3 [60–62], $FAPbI_3$-Br_3-Cl_3 [63–65], $CsPbI_3$-Br_3-Cl_3 [66–68], etc.

[a](Poly([2,6′-4,8-di(5-ethylhexylthienyl)benzo[1,2-b;3,3-b]dithiophene][3-fluoro-2[(2-ethylhexyl)carbonyl]thieno[3,4-b]thiophenediyl])).
[b](Poly(3-hexylthiophene)).
[c](Poly[*N*-9′-heptadecanyl-2,7-carbazole-*alt*-5,5-(4′,7′-di-2-thienyl-2′,1′,3′-benzothiadiazole)], Poly[[9-(1-octylnonyl)-9H-carbazole-2,7-diyl]-2,5-thiophenediyl-2,1,3-benzothiadiazole-4,7-diyl-2,5-thiophenediyl]).
[d](Poly[[4,8-bis[5-(2-ethylhexyl)-4-fluoro-2-thienyl]benzo[1,2-*b*:4,5-*b*′]dithiophene-2,6-diyl]-2,5-thiophenediyl[5,7-bis(2-ethylhexyl)-4,8-dioxo-4*H*,8*H*-benzo[1,2-*c*:4,5-*c*′]dithiophene-1,3-diyl]-2,5-thiophenediyl]).
[e](Poly[(5,6-difluoro-2,1,3-benzothiadiazole-4,7-diyl)).
[f](Poly[[4,8-bis[5-(2-ethylhexyl)-2-thienyl]benzo[1,2-*b*:4,5-*b*′]dithiophene-2,6-diyl]-2,5-thiophenediyl[5,7-bis(2-ethylhexyl)-4,8-dioxo-4*H*,8*H*-benzo[1,2-*c*:4,5-*c*′]dithiophene-1,3-diyl]] polymer).
[g](Poly[2,5-(2-octyldodecyl)-3,6-diketopyrrolopyrrole-alt-5,5-(2,5-di(thien-2-yl)thieno [3,2-b]thiophene)]).
[h](Benzo[1,2-b:4,5-b′]dithiophene).
[i](3,9-bis(2-methylene-((3-(1,1-dicyanomethylene)-6,7-difluoro)-indanone))-5,5,11,11-tetrakis(4-hexylphenyl)-dithieno[2,3-d:2’,3’-d’]-s-indaceno[1,2-b:5,6-b’]dithiophene).
[j](small molecule 1).
[k](small molecule 2).
[l](Phenyl-C61-butyric acid methyl ester).
[m](Phenyl-C71-butyric acid methyl ester).
[n](3,9-bis(2-methylene-(3-(1,1-dicyanomethylene)-indanone))-5,5,11,11-tetrakis(4-hexylphenyl)-dithieno[2,3-d:2′,3′-d′]-s-indaceno[1,2-b:5,6-b′]dithiophene).
[o](2,2′-[[12,13-Bis(2-ethylhexyl)-12,13-dihydro-3,9-diundecylbisthieno[2′′,3′′:4′,5′]thieno[2′,3′:4,5]pyrrolo[3,2-e:2′,3′-g][2,1,3]benzothiadiazole-2,10-diyl]bis[methylidyne(5,6-difluoro-3-oxo-1H-indene-2,1(3H)-diylidene)]]bis[propanedinitrile]).
[p]((5Z,5′Z)-5,5′-((7,7′-(4,4,9,9-tetraoctyl-4,9-dihydro-s-indaceno[1,2-b:5,6-b′]dithiophene-2,7-diyl)bis(benzo[c][1,2,5]thiadiazole-7,4-diyl))bis(methanylylidene))bis(3-ethyl-2-thioxothiazolidin-4-one)).
[q](2,2’-((2Z,2’Z)-((4,4,9,9-tetrahexyl-4,9-dihydro-s-indaceno[1,2-b:5,6-b’]dithiophene-2,7-diyl)bis(methanylylidene))bis(3-oxo-2,3-dihydro-1H-indene-2,1-diylidene))dimalononitrile).
[r](3,9-bis(2-methylene-((3-(1,1-dicyanomethylene)-6/7-methyl)-indanone))-5,5,11,11-tetrakis(4-hexylphenyl)-dithieno[2,3-d:2’,3’-d’]-s-indaceno[1,2-b:5,6-b’]dithiophene).
[s](2,2’-((2Z,2’Z)-(((4,4,9,9-tetrakis(4-hexylphenyl)-4,9-dihydro-sindaceno[1,2-b:5,6-b′]dithiophene-2,7-diyl)bis(4-((2-ethylhexyl)oxy)thiophene-5,2-diyl))bis(methanylylidene))bis(5,6-difluoro-3-oxo-2,3-dihydro-1H-indene-2,1-diylidene))dimalononitrile).
[t](5,5′-[(9,9-Dioctyl-9*H*-fluorene-2,7-diyl)bis(2,1,3-benzothiadiazole-7,4-diylmethylidyne)]bis[3-ethyl-2-thioxo-4-thiazolidinone]).

TABLE 2 | Summarization of the charge transport layer materials.

Type	**Materials**
Electron transport layer	TiO_2 [81], ZnO [82], SnO_2 [83], PCBM[a] [84], Al_2O_3 [85], CdS [86], ZnS [87], LiF [88], etc.
Hole transport layer	PEDOT:PSS[b] [89], MoO_3 [90], Spiro-OMeTAD[c] [91], NiO [92], CuI [93], WS_2 [94], etc.

[a](Phenyl-C61-butyric acid methyl ester).
[b](Poly(2,3-dihydrothieno-1,4-dioxin)-poly(styrenesulfonate)).
[c](2,2′,7,7′-tetrakis[*N*,*N*-di(4-methoxyphenyl)amino]-9,9′-spirobifluorene.

3 | Intrinsic Degradation Mechanisms and Passivation Methods

Intrinsic degradation phenomena in OS and HP-based photoelectrodes can be broadly classified into three categories based on their location. One occurs within the active layer, while the other two occur at the interfaces between the active layer and the HTL and ETL. Firstly, degradation within the active layer is primarily due to photochemical reactions induced by light [101, 102]. This includes the direct decomposition reactions of the light-absorbing material caused by UV light, and structural changes within the active layer resulting from the movement of photoexcited electrons and holes, as well as ion migration induced by light irradiation [103–105]. Secondly, degradation at the interfaces is mainly due to abnormal material and charge transport phenomena occurring at the material interfaces [106]. This includes non-radiative recombination of electrons and holes and corrosion reactions arising from abnormal or incidental

27662098, 2026, 1, Downloaded from https://onlinelibrary.wiley.com/doi/10.1002/EXP.20240020 by CochraneChina, Wiley Online Library on [08/06/2026]. See the Terms and Conditions (https://onlinelibrary.wiley.com/terms-and-conditions) on Wiley Online Library for rules of use; OA articles are governed by the applicable Creative Commons License

reactions at the interfaces [107–109]. Overall, various degradation phenomena can be understood as abnormal reactions occurring near imperfections within the material and at the interfaces [110–112]. Therefore, to address these issues, passivation is required to repair and complement the imperfections in the materials used in the active layer, HTL, and ETL. In this chapter, we will delve into the mechanisms of degradation phenomena occurring at each location and discuss various passivation methods to enhance the operational stability of OS and HP devices.

3.1 | Active Layer

3.1.1 | Organic Semiconductors

In OS-based solar cells and photoelectrodes, a peculiar phenomenon is observed where the device rapidly degrades during the initial few hundred hours, followed by relatively stable operation for several thousand hours. This initial phase of degradation is referred to as "burn-in" and effectively mitigating burn-in is crucial for determining the overall efficiency of the device. Several mechanisms have been proposed to explain this anomaly, including the influence of impurities [113, 114], the crystallinity of organic semiconductor materials [115], and the indirect effects of polymer chain ends [116]. However, the most prominent explanation attributes this phenomenon to the use of fullerene acceptors. It has been reported that fullerenes form dimers through photochemical reactions, creating exciton traps that hinder efficient separation and collection [117, 118].

Consequently, the use of higher adduct fullerene acceptors that do not form dimers, or non-fullerene acceptors (NFAs), can effectively mitigate the burn-in phenomenon and offer higher stability [119, 120]. Indeed, OS-based photoelectrodes utilizing NFAs have shown stable operation without the initial rapid performance decline. Yao et al. reported a photocathode where the acceptor material was changed from fullerene to perylene diimide-based NFA (PDI-V), as shown in Figure 2A [121]. The active layer with NFAs exhibited significantly reduced photogenerated charge accumulation, enabling stable photoelectrode operation for over 12 h. Similarly, Seo et al. developed a photocathode using EH-IDTBR, a representative NFA material, which demonstrated world-class stability for OS-based photoelectrodes [22]. These studies illustrate that effective suppression of initial burn-in significantly impacts the overall stability of OS-based photoelectrodes.

3.1.2 | Halide Perovskites

Early studies conducted by Shao et al. revealed that defects in halide perovskite (HP) materials lead to the formation of high-density deep level traps [124]. The deep level traps not only cause strong non-radiative recombination of charge carriers within the material, leading to a loss of charge carriers in solar cells, but also induce ongoing degradation phenomena within the material [125, 126]. Therefore, to produce highly stable HP-based solar cells and photoelectrodes, it is essential to minimize and suppress defects in HP materials that induce deep level traps through effective passivation methods.

One of the most effective reported techniques is passivation using ionic bonding. This method involves neutralizing specific defect sites with counter ions, and numerous studies have demonstrated that this passivation technique enhances the stability of HP-based devices. Cationic species used as passivating agents can compensate for anionic defects such as undercoordinated I^-, anti-site PbI_3^-, and MA^+ vacancies within HP films. Bi et al. and Abdi-Jalebi et al. reported that small cations like Na^+ and K^+ effectively passivated defects at grain boundaries in HP films, thereby improving photoluminescence quantum yield (PLQY) [127, 128]. Lee et al. reported using a larger cation, phenethylammonium (PEA^+), as a passivating agent for $(HC(NH_2)_2PbI_3)_{0.85}(CH_3NH_3PbBr_3)_{0.15}$ HP-based devices [129]. Observations using Kelvin Probe Force Microscopy (KPFM) indicated that while the grain size decreased, the contact potential difference (CPD) revealed that grain boundaries were passivated with PEA cations, reducing photogenerated charge recombination [130]. This resulted in increased PL intensity, carrier lifetime, and device open-circuit voltage (V_{OC}), effectively reducing degradation phenomena.

Additionally, Krishna et al. applied the short-chain cationic surfactant tetrapropylammonium (TPA^+) to $MAPbI_3$ HP. TPA^+ ions strongly interacted with the perovskite crystal surface, stabilizing uncoordinated halide ions and passivating surface defects, as shown in Figure 2B [122]. X-ray diffraction (XRD) analysis of HP films with TPA^+ revealed that TPA^+ ions interacted with the lead iodide framework, reducing PbI_2 excess and forming a new $TPAPb_4I_9$ phase, as shown in Figure 2C. Although TPA^+ did not integrate into the perovskite lattice, it modified the cell volume and formed TPA^+-rich domains at grain boundaries [131]. This passivated device showed significantly enhanced stability against humidity, temperature, and light stress without external encapsulation, as shown in Figure 2D.

Anionic species can also be used as passivating agents, though their application is less varied. Commonly used methods involve introducing chlorides and iodides, such as $PbCl_2$, NH_4Cl, MACl, FACl, KI, and MAI, to compensate for complementary charge defects like Pb^{2+} and halide vacancies, thus serving passivation roles. However, due to the selective nature of these cationic and anionic passivation methods, recent research has focused on using zwitterions, which possess both positive and negative functional groups. Kim et al. used the L-proline (Pro) zwitterion to passivate $MAPbI_3$ HP films, creating highly efficient and stable HP solar cells and photoelectrodes [123]. Pro, with its positively charged ammonium cation and negatively charged carboxylate anion, effectively neutralized two types of ionic defects in HP films, improving photoluminescence and photovoltage, as shown in Figure 2E. The resulting photoelectrode demonstrated an operational stability exceeding 50 h, one of the best reported at that time, as shown in Figure 2F. This study confirmed that ionic bonding-based passivation positively impacts the operational stability of HP-based devices when used as photoelectrodes.

Interestingly, in addition to ionic bonding-based passivation, various molecular passivation agents have shown improved operational stability and performance in HP films when larger molecules are used [132–134]. This phenomenon occurs because the intercalation of larger molecules disrupts the original 3D structure of HP films, forming 2D or quasi-2D perovskite

27662098, 2026, 1, Downloaded from https://onlinelibrary.wiley.com/doi/10.1002/EXP.20240020 by CochraneChina, Wiley Online Library on [08/06/2026]. See the Terms and Conditions (https://onlinelibrary.wiley.com/terms-and-conditions) on Wiley Online Library for rules of use; OA articles are governed by the applicable Creative Commons License

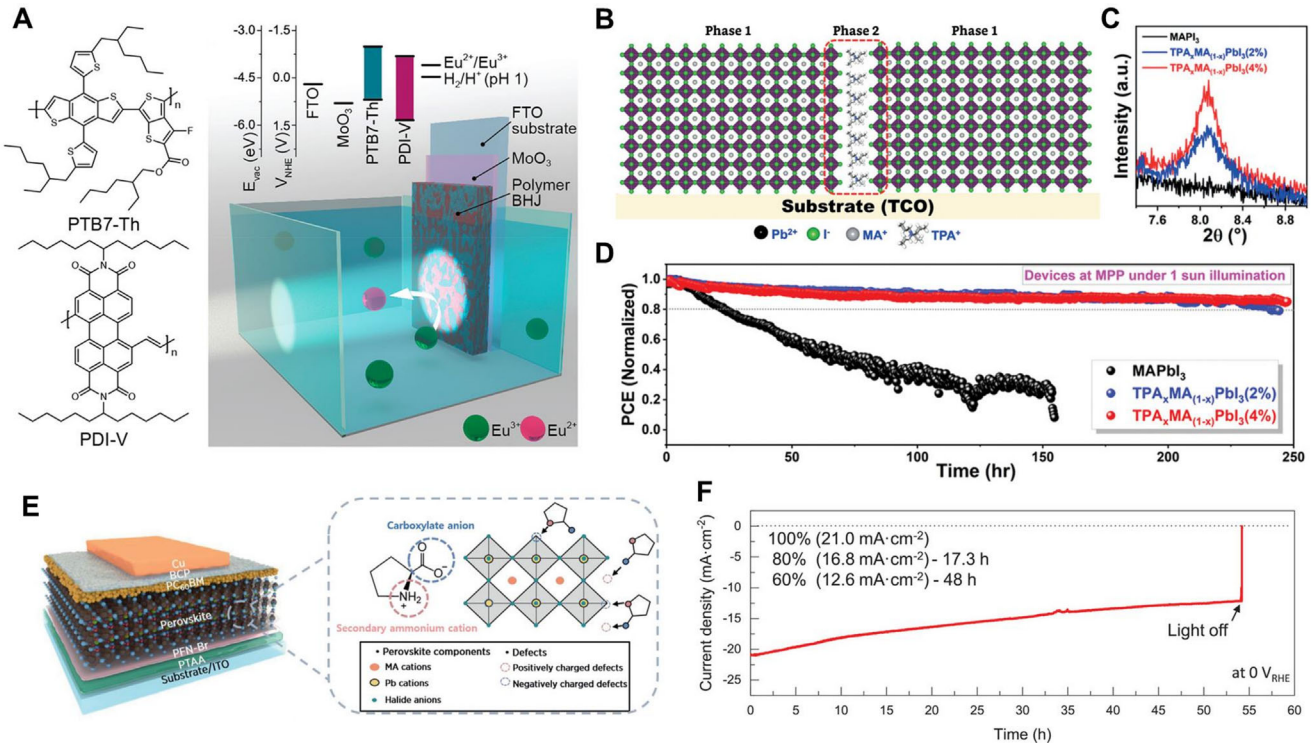


FIGURE 2 | (A) Chemical structures of PTB7-Th polymer donor and PDI-V NFAs, and schematic image of OS-based photocathode. Reproduced with permission [121]. Copyright 2020, American Chemical Society. (B–D) Schematic of perovskite passivation by TPA^+ ion injection, XRD spectra of bare $MAPbI_3$ film and TPA^+ ion treated $MAPbI_3$ films, and operational stability of unencapsulated devices based on $MAPbI_3$, and TPA^+ ion treated $MAPbI_3$. Reproduced with permission [122]. Copyright 2020, Wiley-VCH. (E, F) Schematic image of HP-based photocathode passivated by the Pro zwitterion, and the PEC operational stability of the Pro zwitterion treated HP-based photocathode. Reproduced with permission [123]. Copyright 2021, Wiley-VCH.

structures on the surface and within the film [135–137]. The 2D perovskite structures not only compensate for defects in HP films but also have a wider bandgap compared to the 3D structures, forming type-I heterojunctions at the interfaces [138]. These type-I heterojunctions create electronic barriers that impede charge transport between perovskite grains and between the perovskite and charge transport layers [139, 140]. Consequently, charges reaching the wide-bandgap wrapping layer are reflected back into the bulk, effectively reducing recombination [141]. Recently, intentional mixing of 2D perovskites with 3D perovskites or fabricating layered structures based on this principle has been actively researched [142–145].

3.2 | CTL/Active Layer Interfaces

The HTL must extract holes from the active layer while blocking electrons to prevent recombination of holes and electrons. These two characteristics are intrinsically related to the energy band structure of the HTL. A highest occupied molecular orbital (HOMO) level sufficiently close to the valence band of the active layer allows efficient hole transport. Additionally, the hole mobility in the HTL must be relatively high to minimize charge loss during transport to the contact electrode. However, defects at the HTL/active layer interface paradoxically act as recombination sites for electrons and holes, limiting the hole extraction capability of the HTL. Furthermore, chemical interactions between the HTL and the active layer are another major cause of degradation at the interface. Specifically, ions from the active layer can diffuse into the HTL, or materials from the HTL can penetrate the active layer [146]. These chemical reactions result in structural changes at the interface, causing performance degradation over time. In summary, by preventing defects and anomalies at the HTL/active layer interface, ensuring appropriate energy band alignment and high hole mobility, and enabling smooth hole extraction and electron blocking, the stability of OS and HP-based devices can be enhanced.

Hsiao et al. introduced a sequential passivation strategy with $NiCl_2$ (SPS-$NiCl_2$ treatment) on NiO_x, a representative material for oxide-based HTL, to induce an appropriate gradient in the valence band maximum (VBM) [147]. The SPS-$NiCl_2$ treated NiO_x film had a high Ni^{3+} ratio and low defect density, exhibiting a depth-dependent VBM gradient, as shown in Figure 3. This VBM gradient could be adjusted to achieve proper energy band alignment with the HP film, providing excellent photovoltaic performance and long-term stability for the device. This study demonstrates that aligning the surface elements of the HTL properly can tune the energy alignment (VBM gradient) to match the active layer, offering an effective charge transport path and significantly contributing to improved stability. Ding et al. addressed the thermal instability occurring at the MoO_x and OS active layer interface [148]. They identified that the abnormal oxidation-reduction reactions centered on Cl^- ions of OS material, when directly in contact with MoO_x, were the main cause of degradation and inserted a C_{70} intermediate layer. The C_{70} prevented direct contact between MoO_x and OS, avoiding ion loss and showing remarkable improvement in operational stability.

27662098, 2026, 1, Downloaded from https://onlinelibrary.wiley.com/doi/10.1002/EXP.20240020 by CochraneChina, Wiley Online Library on [08/06/2026]. See the Terms and Conditions (https://onlinelibrary.wiley.com/terms-and-conditions) on Wiley Online Library for rules of use; OA articles are governed by the applicable Creative Commons License

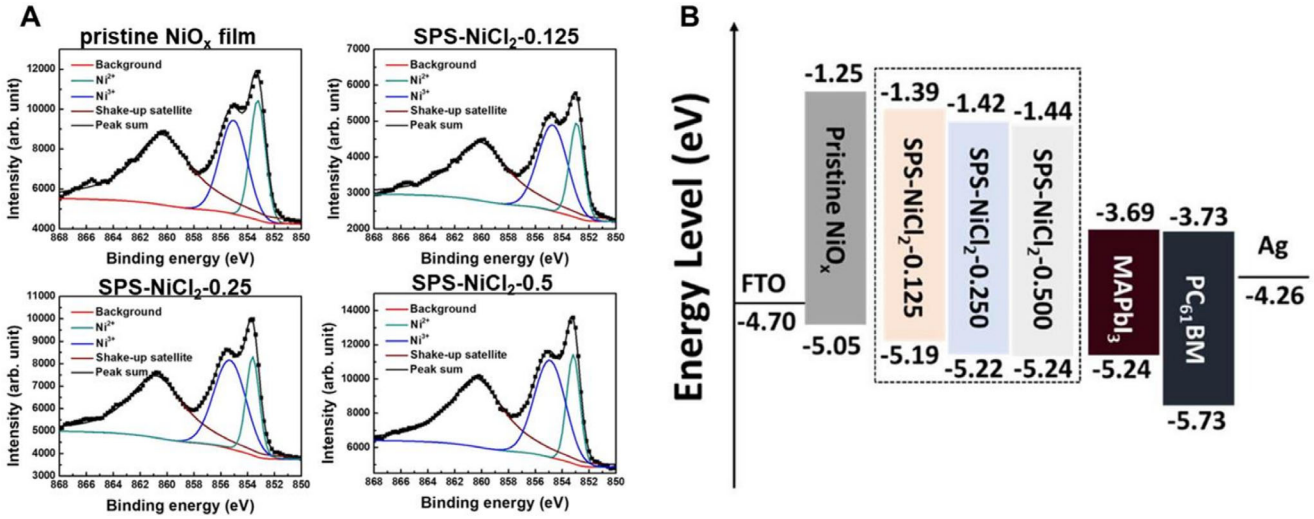


FIGURE 3 | (A) X-ray photoelectron spectra (XPS) of pristine NiO_x film and SPS-$NiCl_2$ treated films. (B) Band alignment of perovskite device with NiO_x and NiO_x with SPS-$NiCl_2$. Reproduced with permission [147]. Copyright 2021, Elsevier.

Degradation at the ETL/active layer interface shows phenomena similar to those at the HTL interface. However, a notable point is that most of the primary materials used in ETL are inorganic metal oxides. This is because the organic ETL materials developed so far do not show satisfactory electron mobility compared to metal oxides, and their energy level alignment is not ideal. These metal oxides inevitably form oxygen vacancies on the surface, which strongly attract electrons, creating fatal trap states and causing severe charge accumulation at the ETL/active layer interface. [149, 150] Kim et al. performed chemical modification using 1,2-ethanedithiol (EDT) to prevent degradation caused by oxygen defects in ZnO ETL [151]. As a result, the suppression of interface defects significantly improved charge collection properties, resulting in increased PCE, and maintained 90% of the initial performance over 1200 h, showing much higher stability compared to ZnO ETL with oxygen defects. Yang et al. developed an ETL by modifying SnO_2 thin film using oxygen radicals to reduce oxygen vacancies at the interface [152]. Oxygen radical passivation formed an SnO_2 surface, which additionally formed hydrogen bonds with HP, improving charge transfer and moisture resistance at the interface (Figure 4A). Thus, long-term operational stability was ensured, and it could be uniformly applied to large-area modules, achieving an efficiency of 18.71%, as shown in Figure 4B,C. Passivating the surface oxygen defects of metal oxide ETLs has been shown to have a remarkably positive impact on device stability.

When using metal oxide CTLs, it is important to note that lattice mismatches can occur at the interface with HP. Lattice mismatches between CTL and HP can create dangling bonds, which naturally lead to deep-level traps and induce additional charge recombination [154–159]. Moreover, lattice mismatches increase ion migration and reduce carrier mobility [160–162]. These issues can be effectively addressed by applying buffer layers. Various materials such as 2D perovskites [163, 164], metal halides [165, 166], and MXene [167, 168] have been used as buffer layers to achieve high-efficiency and stable HP-based devices. Recently, composite technologies have been reported that not only mitigate lattice mismatches but also passivate additional interface bonds. Zhang et al. inserted p-chlorobenzenesulfonic acid (CBSA) self-assembled small-molecule (SASM) at the NiO_x HTL/HP interface to provide dual passivation by alleviating lattice mismatches and compensating for interface defects [153]. The chlorine (—Cl) functional group of SASM bonded with iodine defects of HP, and the sulfonic acid ($—SO_3H$) groups bonded with oxygen vacancies of HTL, thereby suppressing lattice mismatches with an intermediate layer and compensating for surface defects, which were confirmed by XRD and XPS spectra (Figure 4E–G). The HP-based solar cells with dual passivation showed the highest PCE values at the time and exhibited ideal charge behavior over a long period.

Passivating intrinsic degradation is fundamental to the long-term operation of OS and HP-based photoelectrodes. However, intrinsic degradation in OS and HP solar cells and photoelectrodes occurs simultaneously at various locations. Besides the areas described above, degradation can also occur within the CTL [169, 170], at the CTL/electrode interface [171, 172], and within the electrode [173]. Although appropriate passivation methods have been reported to compensate for these issues, further research is needed on passivation materials that can perform multiple functions simultaneously for effective passivation.

4 | Extrinsic Degradation Mechanisms and Passivation Methods

Initial OS and HP-based photoelectrodes exhibited poor stability, failing within an hour, even with passivation against intrinsic degradation [174–177]. These photoelectrodes were created by applying catalysts suitable for PEC reactions on the top electrodes of traditional OS and HP-based solar cell structures. However, the combination of the thin top electrode and catalyst could not prevent electrolyte penetration, leading to extrinsic degradation that caused the structure to dissolve and collapse completely. Consequently, encapsulation methods that could completely block external electrolytes were developed. The first reported technique was metal encapsulation by Crespo-Quesada et al. [33].

27662098, 2026, 1, Downloaded from https://onlinelibrary.wiley.com/doi/10.1002/EXP.20240020 by CochraneChina, Wiley Online Library on [08/06/2026]. See the Terms and Conditions (https://onlinelibrary.wiley.com/terms-and-conditions) on Wiley Online Library for rules of use; OA articles are governed by the applicable Creative Commons License

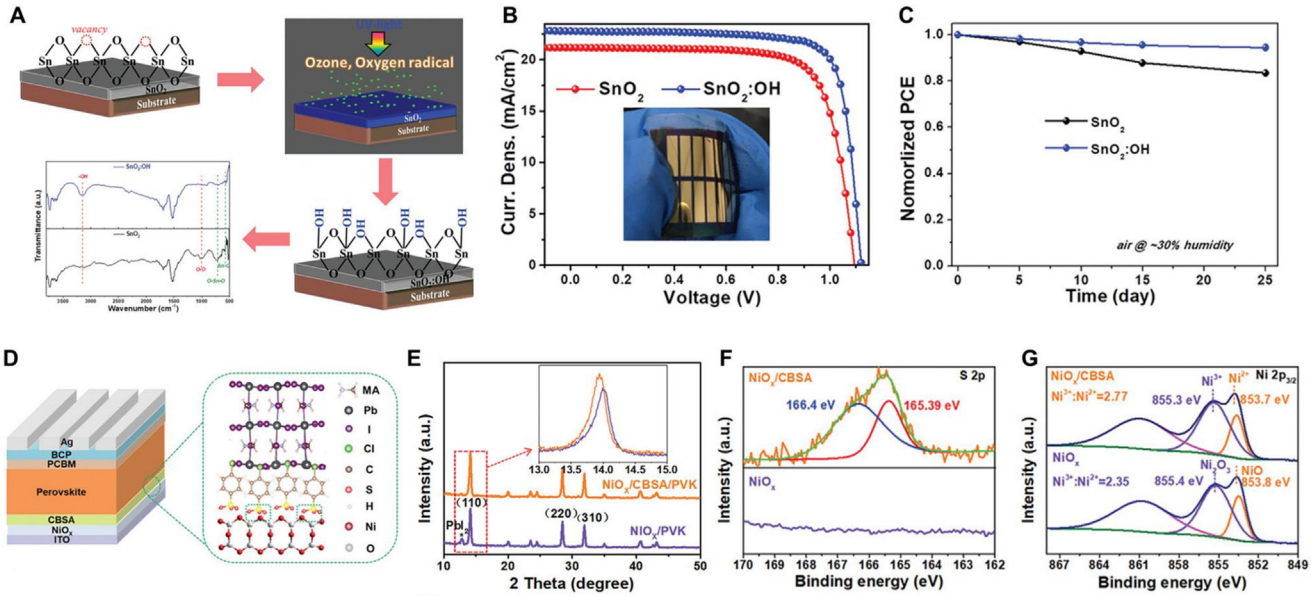


FIGURE 4 | (A–C) Oxygen radical treatment process of SnO_2 films, and the solar cell performances of HP-based devices with SnO_2 and oxygen radical treated SnO_2 film (SnO_2:OH). Reproduced with permission [152]. Copyright 2023, Wiley-VCH. (D–G) Schematic image of PVSCs based on NiO_x/CBSA, and XRD and XPS spectra change corresponding on CBSA treatment. Reproduced with permission [153]. Copyright 2022, Wiley-VCH.

They encapsulated $CH_3NH_3PbI_3$-based HP solar cells with InBiSn alloy, known as Field's metal, and a Pt catalyst (Figure 5A). The InBiSn alloy protected the HP structure from the electrolyte and transferred photogenerated electrons to the catalyst, allowing the HP-based solar cell to operate stably for about 3 h. However, the economic feasibility was unsatisfactory due to the expensive metal materials and noble metal catalysts required for encapsulation. Therefore, researchers began exploring cheaper and more effective encapsulation methods, setting the challenging goal of applying non-noble metal-based catalysts to the top of OS and HP-based solar cells stably.

The proposed solution was to develop an encapsulation part that prevents electrolyte penetration, separate from the OS and HP solar cell device, and use a highly conductive contact material as the adhesion layer. This method adds high flexibility in introducing and synthesizing catalysts in the encapsulation part and can achieve high efficiency with the proper adhesion layer. Thus, the metal-foil encapsulation technique was developed. Unlike conventional metal encapsulation, it used metal-foils with non-noble metal catalysts to fundamentally block electrolyte penetration. Yu et al. reported a photoanode with metal-foil encapsulation technology applied to a PBDB-T:ITIC OS-based solar cell, demonstrating long-term operation in an electrolyte environment, as shown in Figure 5B [178]. They used Ni foil with the high-efficiency non-noble metal catalyst NiFe-LDH as the electrolyte barrier layer and Ga-In eutectic alloy (EGaIn) in the gap between the OS-based solar cell and the metal-foil. This photoanode achieved a current density performance of 15.1 mA cm^{-2} at 1.23 V versus reversible hydrogen electrode (V_{RHE}), which is challenging for conventional oxide-based PEC photoelectrodes, and showed an excellent onset voltage around 0.4 V_{RHE}. Remarkably, it maintained 90% of its initial current density for over 10 h at 1.3 V_{RHE}. EGaIn, as the adhesion layer, not only exhibited high conductivity but also, being a liquid metal, effectively filled the gap between the top electrode of the OS and HP solar cells and the encapsulation layer. The outstanding performance of metal-foil encapsulation using EGaIn and other fusible metals has also been reported in other studies [181–183]. Seo et al. applied Ti-foil and EGaIn as the encapsulation layer and adhesion layer, respectively, to PTB7-Th:EH-IDTBR OS-based solar cells, creating a photocathode that maintained over 90% of its initial current density for 30 h under 0 V_{RHE} conditions, showcasing the world's best operational stability [22]. Choi et al. used a fusible metal adhesion layer with a Ni foil deposited with Fe-doped Ni_3S_2 oxygen evolution reaction catalyst on HP-based solar cells to create a photoanode [184]. This photoanode achieved an applied bias photon-to-current efficiency (ABPE) of 12.79%, the highest among single active layer-based photoanodes, and maintained about 90% of its initial current density for 12 h at 1.23 V_{RHE}.

Additionally, EGaIn proved to be much more stable and efficient as an adhesion layer than Ag paste used in organic solvent-based applications, particularly under conditions where photovoltage is present [123]. However, EGaIn adhesion layers have the drawback of inducing reactions and corrosion with the top electrode of the solar cell to maintain the alloy properties. Over time, the top electrode corrodes, and when the corrosion completes, the contact between the active layer and EGaIn can lead to device failure. Also, the high cost limits its practical application. Therefore, various materials applicable to the adhesion layer have emerged to ensure the ideal encapsulation performance of metal-foil encapsulation.

Recently, carbon-based materials such as graphite epoxy [185, 186], carbon powder [187], carbon paste [188], and commercial adhesive [189] have gained attention due to their low cost and excellent conductivity, which does not significantly degrade the photoelectrode's performance. These materials also react less with the top electrode and encapsulation, significantly contributing to improving the cost-efficiency and operational stability

27662098, 2026, 1, Downloaded from https://onlinelibrary.wiley.com/doi/10.1002/EXP.20240020 by CochraneChina, Wiley Online Library on [08/06/2026]. See the Terms and Conditions (https://onlinelibrary.wiley.com/terms-and-conditions) on Wiley Online Library for rules of use; OA articles are governed by the applicable Creative Commons License

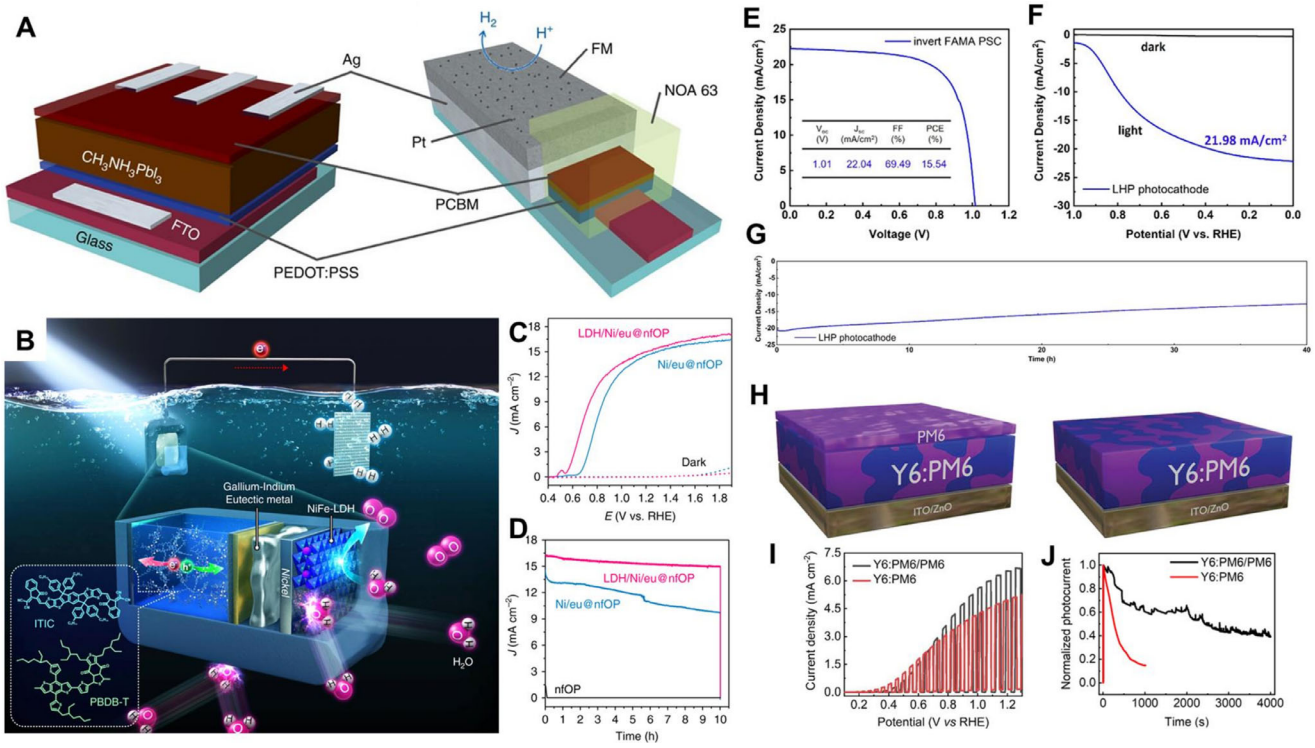


FIGURE 5 | (A) Schematic images of the $MAPbI_3$ HP solar cell and metal-encapsulated HP-based photocathode. Reproduced with permission [33]. Copyright 2016, Springer Nature. (B–D) Schematic image and the PEC performances of metal-foil encapsulated OS-based photoanode with EGaIn adhesion layer. Reproduced with permission [178]. Copyright 2020, Springer Nature. (E–G) The PEC performances of metal-foil encapsulated HP-based photocathode with carbon powder adhesive layer. Reproduced with permission [179]. Copyright 2023, Wiley-VCH. (H–J) Schematic images of polymer overlayer encapsulated OS-based photoanode, and their PEC performances. Reproduced with permission [180]. Copyright 2023, Wiley-VCH.

of OS and HP-based photoelectrodes. Rhee et al. reported HP-based photoanodes and photoanodes using carbon powder as the adhesive layer [179]. The photocurrent density under zero-bias conditions of the completed photoelectrode showed a difference of less than 0.1 mA cm^{-2} from the short-circuit current density of the solar cell, indicating that the relatively low conductivity of the carbon-based adhesive layer hardly affects the overall device performance, as shown in Figure 5E,F. Additionally, the low reactivity of the adhesive layer with the top electrode of the HP solar cell demonstrated excellent operational stability for over 40 h (Figure 5G).

Recent studies have also aimed to replace the encapsulation layer with low-cost materials, considering the practical application of robust encapsulation methods. Examples include carbon-based materials such as graphite sheets [188, 190], carbon paper [189], and carbon plates [191]. An interesting study reported by Jiang et al. used FTO substrates. They connected one side of the FTO substrate to the top electrode of the HP solar cell with Ag paste and exposed the other side with a catalyst [192]. This study demonstrated that easily manufactured and cost-effective conductive oxides are very promising as encapsulation layers.

Finally, a novel study on the encapsulation of OS-based photoelectrodes has been conducted recently. Lee et al. applied a polymer overlayer with high durability in electrolytes directly onto the top of the active layer as an encapsulation layer, as shown in Figure 5H [180]. It not only extended the short photoexcited charge lifetimes of OS-based photoelectrodes but also resolved the operational stability issues of organic materials within electrolytes, previously considered a limitation. Their work not only extended the short photoexcited charge lifetime of OS-based photoelectrodes, but also addressed the issue of operational stability of organic materials in electrolytes, which was previously considered a limitation. The encapsulated photoanodes exhibited higher photocurrent densities than samples without the polymer overlayer and showed a four-fold improvement in stability, as shown in Figure 5I,J. This study significantly impacted the ongoing encapsulation research, indicating that organic-based overlayers could operate more stably from a charge perspective than other inorganic or metal-based overlayers. Thus, designing and applying new molecules more suitable for PEC and electrolyte conditions could further enhance the performance of OS and HP-based photoelectrodes.

5 | PEC Applications of OS and HP Based Photoelectrodes

Applying appropriate passivation and encapsulation has successfully delayed intrinsic and extrinsic degradation in OS and HP-based photoelectrodes. These electrodes, leveraging their excellent inherent photoelectric properties, can contribute significantly to various cases in the PEC field. The high photovoltage and photocurrent density they exhibit provide a different level of PEC reaction efficiency compared to single light-absorbing layer photoelectrodes made from traditional oxides and semiconductor materials. This chapter will explore the practical applications of

27662098, 2026, 1, Downloaded from https://onlinelibrary.wiley.com/doi/10.1002/EXP.20240020 by CochraneChina, Wiley Online Library on [08/06/2026]. See the Terms and Conditions (https://onlinelibrary.wiley.com/terms-and-conditions) on Wiley Online Library for rules of use; OA articles are governed by the applicable Creative Commons License

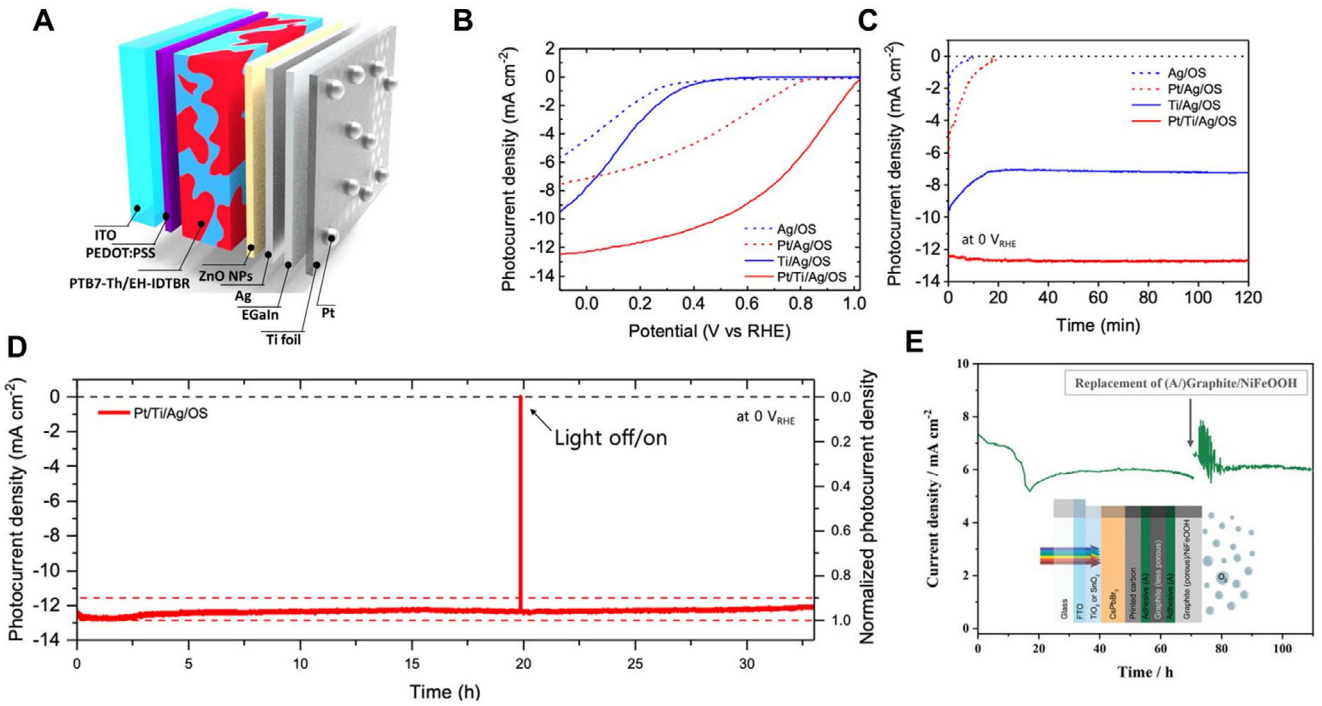


FIGURE 6 | (A–D) Schematic images of the metal-encapsulated OS-based photocathode with EGaIn adhesive layer, and the PEC performances of various encapsulated OS-based photocathodes. Reproduced with permission [22]. Copyright 2022, Royal Society of Chemistry. (E) Long-term operational stability of NiFeOOH/graphite sheet encapsulated HP-based photoanode. Reproduced with permission [190]. Copyright 2023, Wiley-VCH.

OS and HP-based photoelectrodes in the PEC field and discuss the achievements in each area.

5.1 | PEC Water Splitting

PEC water splitting is the most extensively studied topic in the PEC field. In a PEC water splitting system, the cathode is responsible for the hydrogen evolution reaction (HER), and the anode handles the oxygen evolution reaction (OER) [193, 194]. The ultimate goal of this system is to convert solar energy into hydrogen (H_2), a clean and storable energy source, to build a sustainable society. The HER and OER occur at a 2:1 ratio, with the HER consuming 2 electrons and the OER consuming 4 holes. Therefore, both HER and OER must proceed smoothly to develop a high-efficiency system [195–197]. The high absorption coefficients and excellent solar-to-power conversion efficiencies of OS and HP-based photoelectrodes have garnered significant attention in the PEC water splitting field. Consequently, these materials have been actively applied in both photocathode and photoanode areas.

In the field of photocathodes, OS and HP-based photoelectrodes have achieved very high photocurrent densities, on the order of tens of mA cm^{-2}, for the HER at 0 V_{RHE}. Seo et al. developed an OS-based photocathode with metal-foil encapsulation, achieving a remarkable photocurrent density of 12.3 mA cm^{-2} at 0 V_{RHE}, and nearly 100% Faradaic efficiency for HER, indicating that the photoexcited charges were not consumed in degradation reactions within the material but participated in the HER reaction, as shown in Figure 6A–C [22]. The developed photocathode showed less than 10% performance degradation after more than 30 h in 0.5 M H_2SO_4 (pH 1), demonstrating high stability, as shown in Figure 6D. The half-cell solar-to-hydrogen (HC-STH) efficiency reached 5.3%. HP-based photocathodes, which absorb a wider range of wavelengths than OS, have been reported to achieve up to 20 mA cm^{-2} [123, 183, 198].

Photoanodes require more meticulous approaches due to the OER needing twice as many charges as the HER, resulting in slower reaction kinetics [199]. The slow kinetics of OER impose additional stresses like charge accumulation or recombination on the photoanode [200, 201]. To address this, both materials and catalysts need to be enhanced. Yu et al. used a high-performance NiFe-LDH OER catalyst on an OS-based photoanode with metal-foil encapsulation and an EGaIn adhesion layer [178]. When only Ni foil without a catalyst layer was used, the stability of the photoanode decreased. Additionally, considering that stability improved in an electrolyte containing a hole scavenger, which requires fewer holes than the OER, it can be understood that in multi-charge PEC reactions like the OER, the performance of the catalyst significantly impacts the stability of the photoelectrode, in addition to material passivation and encapsulation. Daboczi et al. reported that the highly stable HP-based photoanodes with graphite sheet encapsulation [190]. Phase engineering of the $CsPbBr_3$ HP film reduced intrinsic degradation, and graphite sheets with NiFeOOH catalysts reduced charge accumulation, resulting in 100 h of device failure-free operation, as shown in Figure 6E. This study is a successful application of maximizing photoelectrode operation stability by proper passivation and encapsulation and the introduction of highly efficient HER and OER catalysts.

27662098, 2026, 1, Downloaded from https://onlinelibrary.wiley.com/doi/10.1002/EXP.20240020 by CochraneChina, Wiley Online Library on [08/06/2026]. See the Terms and Conditions (https://onlinelibrary.wiley.com/terms-and-conditions) on Wiley Online Library for rules of use; OA articles are governed by the applicable Creative Commons License

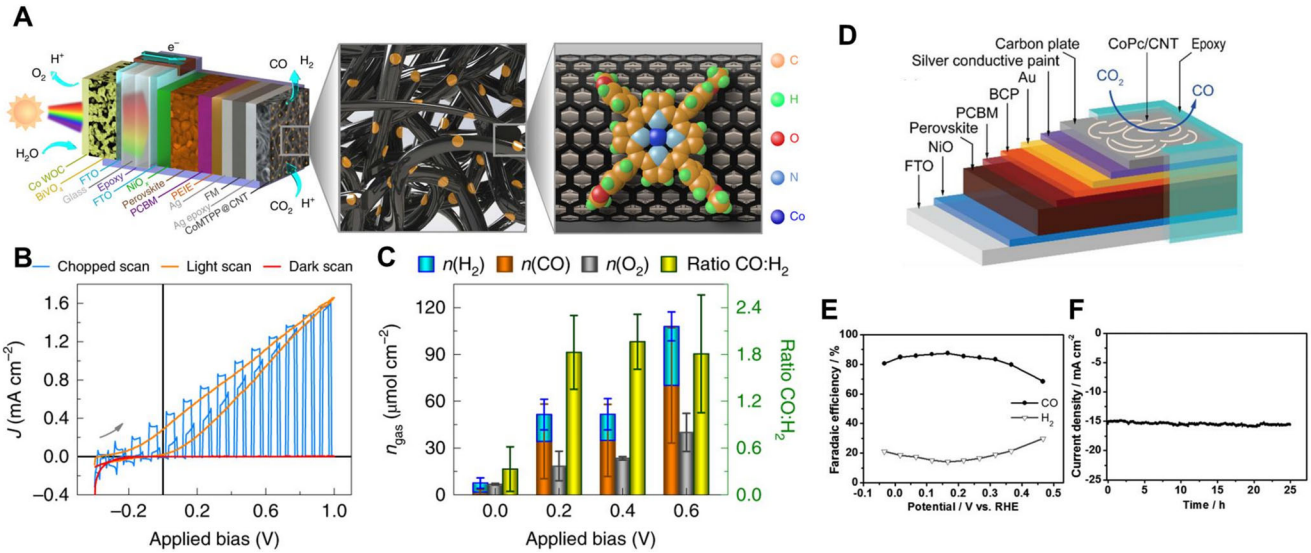


FIGURE 7 | (A–C) Schematic images of the HP-$BiVO_4$ tandem structure, and the PEC CO_2RR performances of HP tandem-based photocathodes. Reproduced with permission [205]. Copyright 2020, Springer Nature. (D–E) Schematic image of CoPc/carbon plate encapsulated HP-based photocathodes, and their PEC CO_2RR performances. Reproduced with permission [191]. Copyright 2020, Wiley-VCH.

5.2 | PEC CO_2 Reduction Reaction

PEC carbon dioxide reduction reaction (CO_2RR) aims to reduce atmospheric CO_2 levels, heightened by fossil fuel usage, by mimicking the carbon cycle process of photosynthesis. Known as artificial photosynthesis, this system focuses on converting excess CO_2 into valuable chemicals such as formic acid (HCOOH), carbon monoxide (CO), methane, methanol (CH_3OH), ethanol (C_2H_5OH), and ethylene (C_2H_4). Key challenges in PEC CO_2RR include addressing the thermodynamic overpotential required for CO_2RR and maintaining selectivity against competing HER [202, 203].

Chen et al. reported that $CH_3NH_3PbI_3$ photoelectrodes encapsulated with $In_{0.4}Bi_{0.6}$ alloy generated sufficient photovoltage to reduce CO_2 to formic acid at −0.6 V_{RHE}, demonstrating the ability of OS and HP-based photoelectrodes to overcome the overpotential for CO_2RR [204]. It was the first result to prove that the high photovoltage and effective photoexcited charge characteristics of OS and HP-based photoelectrodes significantly help in addressing the overpotential required for CO_2RR. Andrei et al. further developed more efficient HP-based photoelectrodes, achieving PEC CO_2RR at 0 V_{RHE} as shown in Figure 7A,B [205]. Also, they fabricated a tandem cell with $BiVO_4$ layer to realize bias-free PEC system, and achieved 1.96 ± 0.35 maximum produced CO:H_2 ratio, as shown in Figure 7C. However, the efficiencies achieved were limited due to the inadequate reaction activity of the catalysts and unsatisfactory performance of the photoelectrodes. Zhang et al. developed a $Cs_{0.15}FA_{0.85}Pb(I_{0.9}Br_{0.1})_3$ photocathode encapsulated with a carbon plate [191]. Carbon plate served as an excellent support for a high-performance molecular CO_2RR catalyst, cobalt phthalocyanine (CoPc), enhancing the photocathode's stability and efficiency, as shown in Figure 7D. The CoPc decorated HP-based photocathode shows the Faradaic efficiency of CO production was 68.4% at 0.47 V_{RHE} and increased to 87.5% at 0.17 V_{RHE} with long-term operational stability for 25 h, as shown in Figure 7D–F. They demonstrated the highest efficiency reported for CO_2 reduction photoelectrodes at the time, emphasizing the importance of selecting appropriate encapsulation layers and catalysts for high-efficiency CO_2RR. However, a more in-depth approach to producing a wider variety of high-value carbon compounds is needed.

5.3 | PEC Ammonia Production

Ammonia (NH_3) is crucial for various industrial applications, particularly as a key component of fertilizers in agriculture [206–208]. However, the traditional Haber–Bosch process for NH_3 production is energy-intensive and heavily reliant on fossil fuels, contributing significantly to greenhouse gas emissions and environmental degradation [209–211]. PEC NH_3 synthesis aims to produce NH_3 in a more sustainable and energy-efficient manner using solar energy, potentially reducing greenhouse gas emissions and overall energy consumption [212–214]. To produce NH_3 via PEC systems, the electrolyte must contain a nitrogen source. Initially, nitrogen gas was purged into the electrolyte, but the low solubility of nitrogen gas and the difficulty of reducing its triple bond limited the yield and Faradaic efficiency [212, 215]. Recent efforts have shifted to using nitrate (NO_3^-) as the nitrogen source, expecting higher efficiency PEC NH_3 production. However, existing photoelectrodes still show limited results, achieving only a few mA cm^{-2} [216, 217].

Tayyebi et al. used $Cs_{0.05}(FA_{0.83}MA_{0.17})_{0.95}Pb(Br_{0.17}I_{0.83})_3$ HP-based photoelectrodes encapsulated with Ni foil and Field's metal to produce NH_3 from NO_3^-, as shown in Figure 7 [218]. They modified the anodic oxidation reaction from OER to glycerol oxidation, reducing the overall system overpotential and achieving bias-free solar-driven NH_3 production with a solar-to-ammonia productivity of 1744.9 ± 20.6 μg cm^{-2} h^{-1}, the highest reported for PEC NH_3 production (Figure 8D). This report demonstrates that HP-based photoelectrodes can significantly impact the yield and efficiency of PEC NH_3 production. The excellent scalability of OS

27662098, 2026, 1, Downloaded from https://onlinelibrary.wiley.com/doi/10.1002/EXP.20240020 by CochraneChina, Wiley Online Library on [08/06/2026]. See the Terms and Conditions (https://onlinelibrary.wiley.com/terms-and-conditions) on Wiley Online Library for rules of use; OA articles are governed by the applicable Creative Commons License

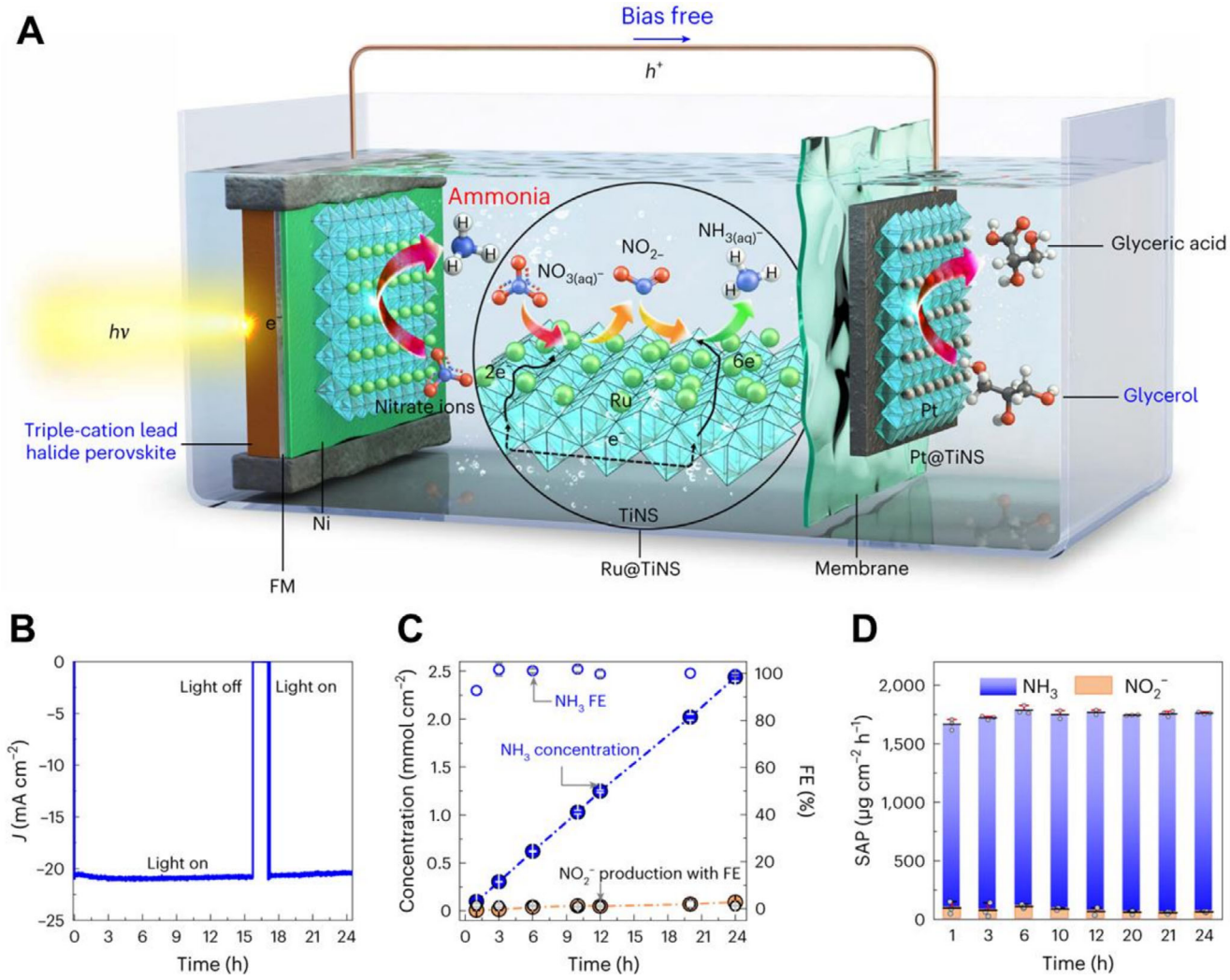


FIGURE 8 | Schematic images of the PEC NH_3 production based on HP-photocathode with glycerol valorization system, and their PEC performances. Reproduced with permission [218]. Copyright 2024, Springer Nature.

and HP materials is expected to further enhance the yield of these high-value-added materials.

5.4 | Bias-Free Systems

The ultimate goal of all PEC research areas is to develop a bias-free PEC system driven solely by photovoltage without an external voltage. Traditional bias-free PEC systems, constructed from low bandgap oxides like $BiVO_4$ and hematite in tandem with Si-based solar cells [219, 220]. They have shown reasonable photovoltage but insufficient to drive PEC systems, with inherently low photocurrent densities necessitating the tandem approach. However, for achieving high efficiency while minimizing system complexity, this approach is less ideal [221, 222]. The excellent photovoltage and charge generation efficiencies of OS and HP materials significantly contribute to this goal [179]. OS and HP-based photoelectrodes achieve around 1.0 V of onset potential shift with a single light-absorbing layer and higher photocurrent densities than oxide photoelectrodes. With various passivation and encapsulation techniques, these materials can operate stably for extended periods. Despite this, achieving bias-free PEC operation with a single photoelectrode remains challenging, leading to the adoption of dual photoelectrode systems using OS and HP materials.

Fehr et al. applied HP photoelectrodes encapsulated with carbon adhesive and graphite sheets to a dual-photoelectrode system, realizing bias-free PEC water splitting [223]. Unlike conventional dual photoelectrode systems, superior photoelectric properties of HP materials resulted in a very high photocurrent density of 20 mA cm^{-2} at one photoelectrode and an outstanding STH efficiency of 12.4 ± 0.7%, as shown in Figure 9A–C. Achieving over 10% STH efficiency is considered the minimum for PEC system commercialization [224]. There HP-based dual-photoelectrode system was one of the first systems to achieve an STH efficiency of over 10%. When these HP materials were connected in tandem with Si solar cells in a conventional bias-free system, they achieved an STH efficiency of approximately 20%, an unprecedented efficiency, and demonstrated commendable stability (Figure 9D–F). This study clearly shows the significant performance gap between the excellent photoelectric properties of OS and HP materials and those of oxide-based photoelectrodes. Choi et al. also reported a bias-free PEC water splitting system

27662098, 2026, 1, Downloaded from https://onlinelibrary.wiley.com/doi/10.1002/EXP.20240020 by CochraneChina, Wiley Online Library on [08/06/2026]. See the Terms and Conditions (https://onlinelibrary.wiley.com/terms-and-conditions) on Wiley Online Library for rules of use; OA articles are governed by the applicable Creative Commons License

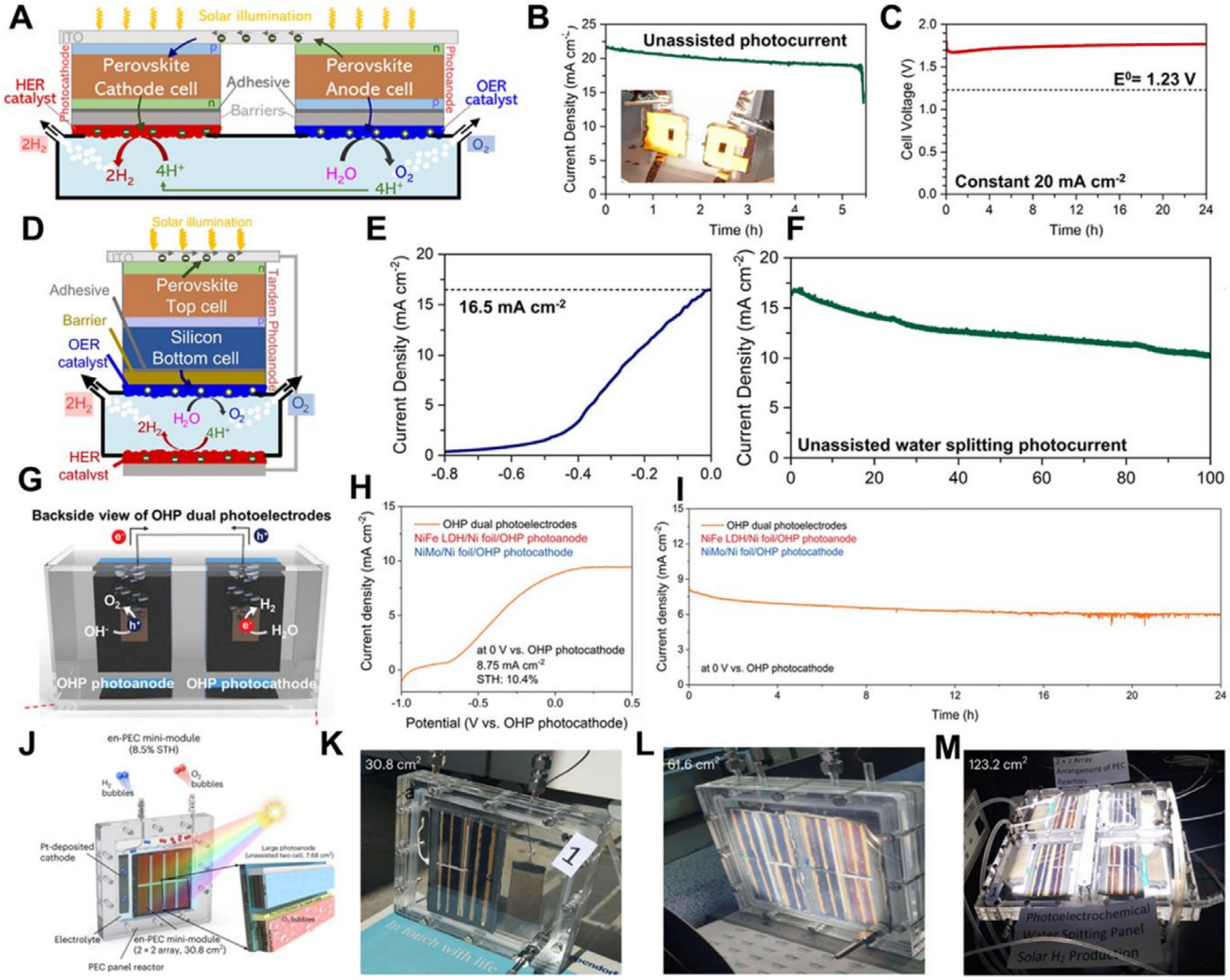


FIGURE 9 | (A–C) Schematic images of the HP based dual-photoelectrodes system for the bias-free water splitting, and their PEC performances. (D–F) Schematic images of the HP/Si tandem-based photoelectrode system for the bias-free water splitting, and their PEC performances. Reproduced with permission [223]. Copyright 2023, Springer Nature. (G–I) Schematic images of the HP based dual-photoelectrodes system with transition metal catalysts for the bias-free water splitting, and their PEC performances. Reproduced with permission [186]. Copyright 2023, Wiley-VCH. (J–M) Schematic images of the HP based-single module photoelectrode, and the photographs of the multi-module photoelectrodes for the bias-free water splitting. Reproduced with permission [225]. Copyright 2024, Springer Nature.

with HP-based dual photoelectrodes with the transition metal catalysts, as shown in Figure 9G–I [186]. They also demonstrated an STH efficiency of over 10%, with the notable achievement of stable operation for 24 h. The excellent stability was attributed to the appropriate use of 2PACz HTL for passivation within the HP solar cell structure, long-term stable encapsulation based on carbon paste, and the great performance of catalysts specifically designed for the electrochemical reactions at both the anode and cathode.

Hansora et al. maximized the scalability of HP materials, achieving a significant technological breakthrough with large-area bias-free PEC water splitting systems, as shown in Figure 9J–M [225]. The research team implemented a range of bias-free PEC water splitting systems, from single devices (0.25 cm^2) to mini modules (30.8 cm^2) and large-scale modules (61.6 cm^2, 123.2 cm^2). They addressed the overpotential required for water splitting solely with HP single devices and single photoelectrodes by connecting the HP solar cells in series and enhanced the current values of the system through parallel connections. As a result, they achieved an STH efficiency of around 10% across all sizes, demonstrating the remarkable commercialization potential of the bias-free PEC system.

6 | Conclusion and Perspectives

In conclusion, next-generation PEC systems leveraging OS and HP hold significant promise for efficient solar energy conversion and environmental pollutant upcycling. These materials offer high photovoltage and impressive current densities, significantly enhancing PEC system performance. However, OS and HP-based photoelectrodes face intrinsic and extrinsic degradation challenges under PEC operating conditions. Intrinsic degradation is driven by photochemical reactions, ion migration, and defects, necessitating various passivation strategies. Extrinsic degradation, caused by electrolyte-induced

27662098, 2026, 1, Downloaded from https://onlinelibrary.wiley.com/doi/10.1002/EXP.20240020 by CochraneChina, Wiley Online Library on [08/06/2026]. See the Terms and Conditions (https://onlinelibrary.wiley.com/terms-and-conditions) on Wiley Online Library for rules of use; OA articles are governed by the applicable Creative Commons License

corrosion and material dissolution, is addressed through advanced encapsulation techniques. These methods ensure the long-term stability of OS and HP-based photoelectrodes, making them viable for diverse PEC applications.

Future research should focus on optimizing the design and synthesis of these materials to enhance their intrinsic stability and performance characteristics. This includes exploring novel organic and perovskite formulations that offer better defect tolerance, increased resistance to photochemical degradation, and improved charge transport properties. Additionally, there is a need to develop more advanced passivation and encapsulation technologies that can provide comprehensive protection against both intrinsic and extrinsic degradation mechanisms. Such advancements could involve multi-functional coatings, hybrid organic-inorganic layers, or self-healing materials that respond dynamically to environmental stressors.

Moreover, scaling up these technologies for practical applications will be crucial for their integration into commercial systems. This involves not only improving material performance but also addressing challenges related to manufacturing, cost, and environmental impact. By advancing these areas, PEC systems based on OS and HP materials could play a pivotal role in sustainable energy solutions, offering efficient pathways for solar-to-chemical energy conversion while simultaneously addressing environmental pollutants such as microplastics, organic dyes, and other hazardous waste products.

By focusing on these key areas of research, the field can make significant strides towards the development of more robust, efficient, and sustainable PEC technologies. These innovations will contribute substantially to the global effort to harness renewable energy sources and mitigate environmental pollution, paving the way for a cleaner, more sustainable future.

Author Contributions

Sanghan Lee supervised the manuscript.

Acknowledgments

This research was supported by the program of Future Hydrogen Original Technology Development (RS-2021-NR057808), through the National Research Foundation of Korea(NRF), funded by the Korean government. (Ministry of Science and ICT(MSIT)). This work was also supported by the National Research Foundation of Korea(NRF) grant funded by the Korea government(MSIT) (No. RS-2025-00563779).

Conflicts of Interest

The authors declare no conflicts of interest.

Data Availability Statement

The data that support the findings of this study are available from the corresponding author upon reasonable request.

References

1. N. S. Lewis and D. G. Nocera, "Powering the Planet: Chemical Challenges in Solar Energy Utilization," *Proceedings of the National Academy of Sciences* 103 (2006): 15729–15735.

2. C. Battaglia, A. Cuevas, and S. De Wolf, "High-Efficiency Crystalline Silicon Solar Cells: Status and Perspectives," *Energy & Environmental Science* 9 (2016): 1552–1576.

3. E. Hawkins, P. Ortega, E. Suckling, et al., "Estimating Changes in Global Temperature Since the Preindustrial Period," *Bulletin of the American Meteorological Society* 98 (2017): 1841–1856.

4. B. D. James, G. N. Baum, J. Perez, and K. N. Baum, DOE Report, Nov. 2009, https://doi.org/10.2172/1218403.

5. H. Nishiyama, T. Yamada, M. Nakabayashi, et al., "Photocatalytic Solar Hydrogen Production From Water on a 100-m2 Scale," *Nature* 598 (2021): 304–307.

6. Y. Pihosh, I. Turkevych, K. Mawatari, et al., "Photocatalytic Generation of Hydrogen by Core-Shell WO3/BiVO4 Nanorods With Ultimate Water Splitting Efficiency," *Scientific Reports* 5 (2015): 11141.

7. Y. Yu, Z. Zhang, X. Yin, et al., "Enhanced Photoelectrochemical Efficiency and Stability Using a Conformal TiO_2 Film on a Black Silicon Photoanode," *Nature Energy* 2 (2017): 17045.

8. M. J. Kenney, M. Gong, Y. Li, et al., "High-Performance Silicon Photoanodes Passivated With Ultrathin Nickel Films for Water Oxidation," *Science* 342 (2013): 836–840.

9. H. Lim, J. L. Young, J. F. Geisz, D. J. Friedman, T. G. Deutsch, and J. Yoon, "High Performance III-V Photoelectrodes for Solar Water Splitting via Synergistically Tailored Structure and Stoichiometry," *Nature Communications* 10 (2019): 3388.

10. Y. Wang, J. Schwartz, J. Gim, R. Hovden, and Z. Mi, "Stable Unassisted Solar Water Splitting on Semiconductor Photocathodes Protected by Multifunctional GaN Nanostructures," *ACS Energy Letters* 4, no. 7 (2019): 1541.

11. K.-Y. Yoon, J. Park, M. Jung, et al., "$NiFeO_x$ Decorated Ge-Hematite/Perovskite for an Efficient Water Splitting System," *Nature Communications* 12 (2021): 4309.

12. B. Zhang, S. Yu, Y. Dai, et al., "Nitrogen-Incorporation Activates $NiFeO_x$ Catalysts for Efficiently Boosting Oxygen Evolution Activity and Stability of $BiVO_4$ Photoanodes," *Nature Communications* 12 (2021): 6969.

13. M. Ma, K. Zhang, P. Li, M. S. Jung, M. J. Jeong, and J. H. Park, "Dual Oxygen and Tungsten Vacancies on a WO3 Photoanode for Enhanced Water Oxidation," *Angewandte Chemie* 128 (2016): 11998–12002.

14. C. Wu, K. Wang, M. Batmunkh, et al., "Multifunctional Nanostructured Materials for Next Generation Photovoltaics," *Nano Energy* 70 (2020): 104480.

15. J. Dai, X. Jiang, H. Wang, and D. Yan, "Organic Photovoltaic Cells With Near Infrared Absorption Spectrum," *Applied Physics Letters* 91, no. 25 (2007): 253503.

16. W. Brütting, *Physics of Organic Semiconductors* (Wiley, 2005).

17. S. De Wolf, J. Holovsky, S.-J. Moon, et al., "Organometallic Halide Perovskites: Sharp Optical Absorption Edge and Its Relation to Photovoltaic Performance," *Journal of Physical Chemistry Letters* 5 (2014): 1035–1039.

18. F. C. Krebs, "Fabrication and Processing of Polymer Solar Cells: A Review of Printing and Coating Techniques," *Solar Energy Materials and Solar Cells* 93 (2009): 394–412.

19. F. Mathies, E. J. List-Kratochvil, and E. L. Unger, "Advances in Inkjet-Printed Metal Halide Perovskite Photovoltaic and Optoelectronic Devices," *Energy Technology* 8 (2020): 1900991.

20. L. Yao, A. Rahmanudin, N. Guijarro, and K. Sivula, "Organic Semiconductor Based Devices for Solar Water Splitting," *Advanced Energy Materials* 8 (2018): 1802585.

21. J. M. Yu, J. Lee, Y. S. Kim, et al., "High-Performance and Stable Photoelectrochemical Water Splitting Cell With Organic-Photoactive-Layer-Based Photoanode," *Nature Communications* 11 (2020): 5509.

22. S. Seo, J.-H. Lee, Y. Kim, et al., "A Long-Term Stable Organic Semiconductor Photocathode-Based Photoelectrochemical Module System

27662098, 2026, 1, Downloaded from https://onlinelibrary.wiley.com/doi/10.1002/EXP.20240020 by CochraneChina, Wiley Online Library on [08/06/2026]. See the Terms and Conditions (https://onlinelibrary.wiley.com/terms-and-conditions) on Wiley Online Library for rules of use; OA articles are governed by the applicable Creative Commons License

for Hydrogen Production," *Journal of Materials Chemistry A* 10 (2022): 13247–13253.

23. J. Yun, H. Lee, Y. S. Park, et al., "Conductive Passivator and Dipole Layer Mixture Enabling High-Performance Stable Perovskite Photoelectrode-Based Solar Water Splitting," *Advanced Energy Materials* 13 (2023): 2301693.

24. H. Zhang, Z. Yang, W. Yu, et al., "A Sandwich-Like Organolead Halide Perovskite Photocathode for Efficient and Durable Photoelectrochemical Hydrogen Evolution in Water," *Advanced Energy Materials* 8 (2018): 1800795.

25. T. Bourgeteau, D. Tondelier, B. Geffroy, et al., "A H_2-Evolving Photocathode Based on Direct Sensitization of MoS_3 With an Organic Photovoltaic Cell," *Energy & Environmental Science* 6 (2013): 2706.

26. H. C. Rojas, S. Bellani, F. Fumagalli, et al., "Polymer-Based Photocathodes With a Solution-Processable Cuprous Iodide Anode Layer and a Polyethyleneimine Protective Coating," *Energy & Environmental Science* 9 (2016): 3710–3723.

27. P. Da, M. Cha, L. Sun, Y. Wu, Z.-S. Wang, and G. Zheng, "High-Performance Perovskite Photoanode Enabled by Ni Passivation and Catalysis," *Nano Letters* 15 (2015): 3452–3457.

28. C. Wang, S. Yang, X. Chen, T. Wen, and H. G. Yang, "Surface-Functionalized Perovskite Films for Stable Photoelectrochemical Water Splitting," *Journal of Materials Chemistry A* 5 (2017): 910–913.

29. M. Grätzel, "Photoelectrochemical Cells," *Nature* 414 (2001): 338–344.

30. F. Nandjou and S. Haussener, "Degradation in Photoelectrochemical Devices: Review With an Illustrative Case Study," *Journal of Physics D: Applied Physics* 50 (2017): 124002.

31. D. Bi, X. Li, J. V. Milić, et al., "Multifunctional Molecular Modulators for Perovskite Solar Cells With Over 20% Efficiency and High Operational Stability," *Nature Communications* 9 (2018): 4482.

32. B. Philippe, B.-W. Park, R. Lindblad, et al., "Chemical and Electronic Structure Characterization of Lead Halide Perovskites and Stability Behavior Under Different Exposures—A Photoelectron Spectroscopy Investigation," *Chemistry of Materials* 27 (2015): 1720–1731.

33. M. Crespo-Quesada, L. M. Pazos-Outón, J. Warnan, M. F. Kuehnel, R. H. Friend, and E. Reisner, "Metal-Encapsulated Organolead Halide Perovskite Photocathode for Solar-Driven Hydrogen Evolution in Water," *Nature Communications* 7 (2016): 12555.

34. J. H. Kim, D. Hansora, P. Sharma, J.-W. Jang, and J. S. Lee, "Toward Practical Solar Hydrogen Production—An Artificial Photosynthetic Leaf-to-Farm Challenge," *Chemical Society Reviews* 48 (2019): 1908–1971.

35. R. Tao, Z. Sun, F. Li, W. Fang, and L. Xu, "Achieving Organic Metal Halide Perovskite into a Conventional Photoelectrode: Outstanding Stability in Aqueous Solution and High-Efficient Photoelectrochemical Water Splitting," *ACS Applied Energy Materials* 2 (2019): 1969–1976.

36. J. D. Servaites, M. A. Ratner, and T. J. Marks, "Organic Solar Cells: A New Look at Traditional Models," *Energy & Environmental Science* 4 (2011): 4410.

37. S. Wang, T. Sakurai, W. Wen, and Y. Qi, "Energy Level Alignment at Interfaces in Metal Halide Perovskite Solar Cells," *Advanced Materials Interfaces* 5 (2018): 1800260.

38. H. Hoppe and N. S. Sariciftci, "Organic Solar Cells: An Overview," *Journal of Materials Research* 19 (2004): 1924–1945.

39. W.-J. Yin, J.-H. Yang, J. Kang, Y. Yan, and S.-H. Wei, "Halide Perovskite Materials for Solar Cells: A Theoretical Review," *Journal of Materials Chemistry A* 3 (2015): 8926–8942.

40. C. C. Chueh, S. C. Chien, H. L. Yip, et al., "Toward High-Performance Semi-Transparent Polymer Solar Cells: Optimization of Ultra-Thin Light Absorbing Layer and Transparent Cathode Architecture," *Advanced Energy Materials* 3 (2013): 417–423.

41. T. Wu, D. Cui, X. Liu, et al., "Efficient and Stable Tin Perovskite Solar Cells Enabled by Graded Heterostructure of Light-Absorbing Layer," *Solar RRL* 4 (2020): 2000240.

42. S. Holliday, R. S. Ashraf, A. Wadsworth, et al., "High-Efficiency and Air-Stable P3HT-Based Polymer Solar Cells With a New Non-Fullerene Acceptor," *Nature Communications* 7 (2016): 11585.

43. X. Yi, B. Gautam, I. Constantinou, et al., "Impact of Nonfullerene Molecular Architecture on Charge Generation, Transport, and Morphology in PTB7-Th-Based Organic Solar Cells," *Advanced Functional Materials* 28 (2018): 1802702.

44. J. W. Kingsley, P. P. Marchisio, H. Yi, et al., "Molecular Weight Dependent Vertical Composition Profiles of PCDTBT:PC71BM Blends for Organic Photovoltaics," *Scientific Reports* 4 (2014): 5286.

45. M.-A. Pan, T.-K. Lau, Y. Tang, et al., "16.7%-Efficiency Ternary Blended Organic Photovoltaic Cells With PCBM as the Acceptor Additive to Increase the Open-Circuit Voltage and Phase Purity," *Journal of Materials Chemistry A* 7 (2019): 20713–20722.

46. J. Zhang, W. Liu, M. Zhang, S. Xu, F. Liu, and X. Zhu, "PCE11-Based Polymer Solar Cells With High Efficiency Over 13% Achieved by Room-Temperature Processing," *Journal of Materials Chemistry A* 8 (2020): 8661–8668.

47. S. Lee, K. H. Park, J. H. Lee, et al., "Achieving Thickness-Insensitive Morphology of the Photoactive Layer for Printable Organic Photovoltaic Cells via Side Chain Engineering in Nonfullerene Acceptors," *Advanced Energy Materials* 9 (2019): 1900044.

48. S. Liu, P. You, J. Li, et al., "Enhanced Efficiency of Polymer Solar Cells by Adding a High-Mobility Conjugated Polymer," *Energy & Environmental Science* 8 (2015): 1463–1470.

49. M. Li, W. Ni, X. Wan, Q. Zhang, B. Kan, and Y. Chen, "Benzo[1,2-b:4,5-b′]Dithiophene (BDT)-Based Small Molecules for Solution Processed Organic Solar Cells," *Journal of Materials Chemistry A* 3 (2015): 4765–4776.

50. H. Dahiya, V. Cuesta, P. de la Cruz, F. Langa, and G. D. Sharma, "Highly Efficient (15.08%) All-Small-Molecule Ternary Solar Cells Constructed With a Porphyrin as a Donor and Two Acceptors," *ACS Applied Energy Materials* 4 (2021): 4498–4506.

51. O. Alqahtani, M. Babics, J. Gorenflot, et al., "Mixed Domains Enhance Charge Generation and Extraction in Bulk-Heterojunction Solar Cells With Small-Molecule Donors," *Advanced Energy Materials* 8 (2018): 1702941.

52. L. Zeng, C. W. Tang, and S. H. Chen, "Effects of Active Layer Thickness and Thermal Annealing on Polythiophene: Fullerene Bulk Heterojunction Photovoltaic Devices," *Applied Physics Letters* 97, no. 5 (2010): 053305.

53. J. Lee, J.-H. Lee, H. Yao, et al., "Efficient and Photostable Ternary Organic Solar Cells With a Narrow Band Gap Non-fullerene Acceptor and Fullerene Additive," *Journal of Materials Chemistry A* 8 (2020): 6682–6691.

54. K. Cnops, B. P. Rand, D. Cheyns, and P. Heremans, "Enhanced Photocurrent and Open-Circuit Voltage in a 3-Layer Cascade Organic Solar Cell," *Applied Physics Letters* 101 (2012): 143301.

55. K. Weng, L. Ye, L. Zhu, et al., "Optimized Active Layer Morphology Toward Efficient and Polymer Batch Insensitive Organic Solar Cells," *Nature Communications* 11 (2020): 2855.

56. M. H. Elsayed, B.-H. Jiang, Y.-P. Wang, et al., "Indacenodithiophene-Based N-type Conjugated Polymers Provide Highly Thermally Stable Ternary Organic Photovoltaics Displaying a Performance of 17.5%," *Journal of Materials Chemistry A* 9 (2021): 9780–9790.

57. W. Li, J. Cai, Y. Yan, et al., "Correlating Three-Dimensional Morphology With Function in PBDB-T:IT-M Non-Fullerene Organic Solar Cells," *Solar RRL* 2 (2018): 1800114.

58. N. Chaturvedi, N. Gasparini, D. Corzo, et al., "All Slot-Die Coated Non-Fullerene Organic Solar Cells With PCE 11%," *Advanced Functional Materials* 31 (2021): 2009996.

27662098, 2026, 1, Downloaded from https://onlinelibrary.wiley.com/doi/10.1002/EXP.20240020 by CochraneChina, Wiley Online Library on [08/06/2026]. See the Terms and Conditions (https://onlinelibrary.wiley.com/terms-and-conditions) on Wiley Online Library for rules of use; OA articles are governed by the applicable Creative Commons License

59. S. Holliday, R. S. Ashraf, C. B. Nielsen, et al., "A Rhodanine Flanked Nonfullerene Acceptor for Solution-Processed Organic Photovoltaics," *Journal of the American Chemical Society* 137 (2015): 898–904.

60. Y. Wu, F. Xie, H. Chen, et al., "Thermally Stable MAPbI 3 Perovskite Solar Cells With Efficiency of 19.19% and Area Over 1 cm^2 Achieved by Additive Engineering," *Advanced Materials* 29 (2017): 1701073.

61. S. Ryu, J. H. Noh, N. J. Jeon, et al., "Voltage Output of Efficient Perovskite Solar Cells With High Open-Circuit Voltage and Fill Factor," *Energy & Environmental Science* 7 (2014): 2614–2618.

62. W. Zhou, P. Zhou, X. Lei, et al., "Phase Engineering of Perovskite Materials for High-Efficiency Solar Cells: Rapid Conversion of $CH_3NH_3PbI_3$ to Phase-Pure $CH_3NH_3PbCl_3$ via Hydrochloric Acid Vapor Annealing Post-Treatment," *ACS Applied Materials & Interfaces* 10 (2018): 1897–1908.

63. H. Lu, Y. Liu, P. Ahlawat, et al., "Vapor-Assisted Deposition of Highly Efficient, Stable Black-Phase $FAPbI_3$ Perovskite Solar Cells," *Science* 370 (2020): eabb8985.

64. N. Arora, M. I. Dar, M. Abdi-Jalebi, et al., "Intrinsic and Extrinsic Stability of Formamidinium Lead Bromide Perovskite Solar Cells Yielding High Photovoltage," *Nano Letters* 16 (2016): 7155–7162.

65. S. Govinda, B. P. Kore, D. Swain, et al., "Critical Comparison of $FAPbX_3$ and $MAPbX_3$ (X = Br and Cl): How Do They Differ?," *Journal of Physical Chemistry C* 122 (2018): 13758–13766.

66. J. Duan, Y. Zhao, B. He, and Q. Tang, "Simplified Perovskite Solar Cell With 4.1% Efficiency Employing Inorganic $CsPbBr_3$ as Light Absorber," *Small* 14 (2018): 1704443.

67. W. Ahmad, J. Khan, G. Niu, and J. Tang, "Inorganic $CsPbI_3$ Perovskite-Based Solar Cells: A Choice for a Tandem Device," *Solar RRL* 1 (2017): 1700048.

68. Q. Wang, X. Zhang, Z. Jin, et al., "Energy-Down-Shift $CsPbCl_3$: Mn Quantum Dots for Boosting the Efficiency and Stability of Perovskite Solar Cells," *ACS Energy Letters* 2 (2017): 1479–1486.

69. A. J. Heeger, "25th Anniversary Article: Bulk Heterojunction Solar Cells: Understanding the Mechanism of Operation," *Advanced Materials* 26 (2014): 10–28.

70. G. Dennler, M. C. Scharber, and C. J. Brabec, "Polymer-Fullerene Bulk-Heterojunction Solar Cells," *Advanced Materials* 21 (2009): 1323–1338.

71. S. H. Park, A. Roy, S. Beaupré, et al., "Bulk Heterojunction Solar Cells With Internal Quantum Efficiency Approaching 100%," *Nature Photon* 3 (2009): 297–302.

72. J. K. Lee, W. L. Ma, C. J. Brabec, et al., "Processing Additives for Improved Efficiency From Bulk Heterojunction Solar Cells," *Journal of the American Chemical Society* 130 (2008): 3619–3623.

73. L. Lang, J.-H. Yang, H.-R. Liu, H. Xiang, and X. Gong, "First-Principles Study on the Electronic and Optical Properties of Cubic ABX_3 Halide Perovskites," *Physics Letters A* 378 (2014): 290–293.

74. V. M. Goldschmidt, "Die Gesetze der Krystallochemie," *Die Naturwissenschaften* 14 (1926): 477–485.

75. Y. Yuan, R. Xu, H.-T. Xu, F. Hong, F. Xu, and L.-J. Wang, "Nature of the Band Gap of Halide Perovskites ABX3 (A = CH_3NH_3 , Cs; B = Sn, Pb; X = Cl, Br, I): First-Principles Calculations," *Chinese Physics B* 24 (2015): 116302.

76. G. Yang, H. Tao, P. Qin, W. Ke, and G. Fang, "Recent Progress in Electron Transport Layers for Efficient Perovskite Solar Cells," *Journal of Materials Chemistry A* 4 (2016): 3970–3990.

77. M. F. M. Noh, C. H. Teh, R. Daik, et al., "Laser-Irradiated Inclined Metal Nanocolumns for Selective, Scalable, and Room-Temperature Synthesis of Plasmonic Isotropic Nanospheres," *Journal of Materials Chemistry C* 6 (2018): 6038–6045.

78. K. Mahmood, S. Sarwar, and M. T. Mehran, "Current Status of Electron Transport Layers in Perovskite Solar Cells: Materials and Properties," *RSC Advances* 7 (2017): 17044–17062.

79. X. Zhang, H. Zhang, Y. Li, et al., "Recent Progress in Hole-Transporting Layers of Conventional Organic Solar Cells With P–I–N Structure," *Advanced Functional Materials* 32 (2022): 2205398.

80. Y. Yao, C. Cheng, C. Zhang, H. Hu, K. Wang, and S. De Wolf, "Organic Hole-Transport Layers for Efficient, Stable, and Scalable Inverted Perovskite Solar Cells," *Advanced Materials* 34 (2022): 2203794.

81. M. M. Tavakoli, P. Yadav, R. Tavakoli, and J. Kong, "Surface Engineering of TiO_2 ETL for Highly Efficient and Hysteresis-Less Planar Perovskite Solar Cell (21.4%) With Enhanced Open-Circuit Voltage and Stability," *Advanced Energy Materials* 8 (2018): 1800794.

82. H. Wang, S. Cao, B. Yang, et al., "NH_4 Cl-Modified ZnO for High-Performance $CsPbIBr_2$ Perovskite Solar Cells via Low-Temperature Process," *Solar RRL* 4 (2020): 1900363.

83. Q. Jiang, X. Zhang, and J. You, "SnO_2: A Wonderful Electron Transport Layer for Perovskite Solar Cells," *Small* 14 (2018): 1801154.

84. D. Yang, X. Zhang, K. Wang, et al., "Stable Efficiency Exceeding 20.6% for Inverted Perovskite Solar Cells Through Polymer-Optimized PCBM Electron-Transport Layers," *Nano Letters* 19 (2019): 3313–3320.

85. T. Mahmoudi, Y. Wang, and Y. B. Hahn, "$SrTiO_3/Al_2O_3$-Graphene Electron Transport Layer for Highly Stable and Efficient Composites-Based Perovskite Solar Cells With 20.6% Efficiency," *Advanced Energy Materials* 10 (2020): 1903369.

86. C. D. Wessendorf, J. Hanisch, D. Müller, and E. Ahlswede, "CdS as Electron Transport Layer for Low-Hysteresis Perovskite Solar Cells," *Solar RRL* 2 (2018): 1800056.

87. R. Chen, J. Cao, Y. Duan, et al., "High-Efficiency, Hysteresis-Less, UV-Stable Perovskite Solar Cells With Cascade ZnO–ZnS Electron Transport Layer," *Journal of the American Chemical Society* 141 (2018): 541–547.

88. L. Chen, C. Xu, W. Hu, et al., "Improving the Electrical Performance of Inverted Perovskite Solar Cell With LiF Anode Buffer Layer," *Organic Electronics* 101 (2022): 106401.

89. F. J. Lim, K. Ananthanarayanan, J. Luther, and G. W. Ho, "Influence of a Novel Fluorosurfactant Modified PEDOT:PSS Hole Transport Layer on the Performance of Inverted Organic Solar Cells," *Journal of Materials Chemistry* 22 (2012): 25057.

90. Y.-J. Lee, J. Yi, G. F. Gao, et al., "Low-Temperature Solution-Processed Molybdenum Oxide Nanoparticle Hole Transport Layers for Organic Photovoltaic Devices," *Advanced Energy Materials* 2, no. 10 (2012): 1193.

91. W. H. Nguyen, C. D. Bailie, E. L. Unger, and M. D. McGehee, "Enhancing the Hole-Conductivity of Spiro-OMeTAD Without Oxygen or Lithium Salts by Using $Spiro(TFSI)_2$ in Perovskite and Dye-Sensitized Solar Cells," *Journal of the American Chemical Society* 136 (2014): 10996–11001.

92. M. B. Islam, M. Yanagida, Y. Shirai, Y. Nabetani, and K. Miyano, "NiO_X Hole Transport Layer for Perovskite Solar Cells With Improved Stability and Reproducibility," *ACS Omega* 2 (2017): 2291–2299.

93. A. Liu, H. Zhu, M.-G. Kim, J. Kim, and Y.-Y. Noh, "Engineering Copper Iodide (CuI) for Multifunctional p-Type Transparent Semiconductors and Conductors," *Advancement of Science* 8 (2021): 2100546.

94. Y. Lin, B. Adilbekova, Y. Firdaus, et al., "17% Efficient Organic Solar Cells Based on Liquid Exfoliated WS_2 as a Replacement for PEDOT:PSS," *Advanced Materials* 31 (2019): 1902965.

95. M. W. Rowell and M. D. McGehee, "Transparent Electrode Requirements for Thin Film Solar Cell Modules," *Energy & Environmental Science* 4 (2011): 131–134.

96. W. Ming, D. Yang, T. Li, L. Zhang, and M.-H. Du, "Formation and Diffusion of Metal Impurities in Perovskite Solar Cell Material CH_3 NH_3PbI_3: Implications on Solar Cell Degradation and Choice of Electrode," *Advancement of Science* 5 (2018): 1700662.

97. A. Hauch and A. Georg, "Diffusion in the Electrolyte and Charge-Transfer Reaction at the Platinum Electrode in Dye-Sensitized Solar Cells," *Electrochimica Acta* 46 (2001): 3457–3466.

27662098, 2026, 1, Downloaded from https://onlinelibrary.wiley.com/doi/10.1002/EXP.20240020 by CochraneChina, Wiley Online Library on [08/06/2026]. See the Terms and Conditions (https://onlinelibrary.wiley.com/terms-and-conditions) on Wiley Online Library for rules of use; OA articles are governed by the applicable Creative Commons License

98. E. M. Sanehira, B. J. Tremolet de Villers, P. Schulz, et al., "Influence of Electrode Interfaces on the Stability of Perovskite Solar Cells: Reduced Degradation Using MoO_X/Al for Hole Collection," *ACS Energy Letters* 1 (2016): 38–45.

99. J. Chen, D. Lee, and N.-G. Park, "Stabilizing the Ag Electrode and Reducing J—V Hysteresis Through Suppression of Iodide Migration in Perovskite Solar Cells," *ACS Applied Materials & Interfaces* 9 (2017): 36338–36349.

100. Z. A. Page, Y. Liu, V. V. Duzhko, T. P. Russell, and T. Emrick, "Fulleropyrrolidine Interlayers: Tailoring Electrodes to Raise Organic Solar Cell Efficiency," *Science* 346 (2014): 441–444.

101. D. E. Motaung, G. F. Malgas, and C. J. Arendse, "Insights Into the Stability and Thermal Degradation of P3HT:C60 Blended Films for Solar Cell Applications," *Journal of Materials Science* 46 (2011): 4942–4952.

102. S.-W. Lee, S. Kim, S. Bae, et al., "UV Degradation and Recovery of Perovskite Solar Cells," *Scientific Reports* 6 (2016): 38150.

103. J. U. Lee, J. W. Jung, J. W. Jo, and W. H. Jo, "Degradation and Stability of Polymer-Based Solar Cells," *Journal of Materials Chemistry* 22 (2012): 24265.

104. A. Classen, T. Heumueller, I. Wabra, et al., "Revealing Hidden UV Instabilities in Organic Solar Cells by Correlating Device and Material Stability," *Advanced Energy Materials* 9 (2019): 1902124.

105. K. Domanski, B. Roose, T. Matsui, et al., "Migration of Cations Induces Reversible Performance Losses Over Day/Night Cycling in Perovskite Solar Cells," *Energy & Environmental Science* 10 (2017): 604–613.

106. S. Rafique, S. M. Abdullah, K. Sulaiman, and M. Iwamoto, "Fundamentals of Bulk Heterojunction Organic Solar Cells: An Overview of Stability/Degradation Issues and Strategies for Improvement," *Renewable Sustainable Energy Reviews* 84 (2018): 43–53.

107. S. D. Stranks, "Nonradiative Losses in Metal Halide Perovskites," *ACS Energy Letters* 2 (2017): 1515–1525.

108. L. M. Pazos-Outón, T. P. Xiao, and E. Yablonovitch, "Fundamental Efficiency Limit of Lead Iodide Perovskite Solar Cells," *Journal of Physical Chemistry Letters* 9 (2018): 1703–1711.

109. J. C. Blakesley and D. Neher, "Relationship Between Energetic Disorder and Open-Circuit Voltage in Bulk Heterojunction Organic Solar Cells," *Physical Review B* 84 (2011): 075210.

110. B. Chen, P. N. Rudd, S. Yang, Y. Yuan, and J. Huang, "Imperfections and Their Passivation in Halide Perovskite Solar Cells," *Chemical Society Reviews* 48 (2019): 3842–3867.

111. S. Heo, G. Seo, Y. Lee, et al., "Deep Level Trapped Defect Analysis in $CH_3NH_3PbI_3$ Perovskite Solar Cells by Deep Level Transient Spectroscopy," *Energy & Environmental Science* 10 (2017): 1128–1133.

112. S. Heo, G. Seo, Y. Lee, et al., "Origins of High Performance and Degradation in the Mixed Perovskite Solar Cells," *Advanced Materials* 31 (2019): 1805438.

113. R. S. Ashraf, B. C. Schroeder, H. A. Bronstein, et al., "The Influence of Polymer Purification on Photovoltaic Device Performance of a Series of Indacenodithiophene Donor Polymers," *Advanced Materials* 25 (2013): 2029–2034.

114. R. F. Salzman, J. Xue, B. P. Rand, A. Alexander, M. E. Thompson, and S. R. Forrest, "The Effects of Copper Phthalocyanine Purity on Organic Solar Cell Performance," *Organic Electronics* 6 (2005): 242–246.

115. T. Heumueller, W. R. Mateker, I. T. Sachs-Quintana, et al., "Reducing Burn-In Voltage Loss in Polymer Solar Cells by Increasing the Polymer Crystallinity," *Energy & Environmental Science* 7 (2014): 2974–2980.

116. C. Bracher, H. Yi, N. W. Scarratt, et al., "The Effect of Residual Palladium Catalyst on the Performance and Stability of PCDTBT:PC70BM Organic Solar Cells," *Organic Electronics* 27 (2015): 266–273.

117. Q. Burlingame, X. Tong, J. Hankett, M. Slootsky, Z. Chen, and S. R. Forrest, "Photochemical Origins of Burn-In Degradation in Small Molecular Weight Organic Photovoltaic Cells," *Energy & Environmental Science* 8 (2015): 1005–1010.

118. A. Distler, T. Sauermann, H.-J. Egelhaaf, et al., "The Effect of PCBM Dimerization on the Performance of Bulk Heterojunction Solar Cells," *Advanced Energy Materials* 4 (2014): 1300693.

119. A. Distler, T. Sauermann, H. J. Egelhaaf, et al., "The Effect of PCBM Dimerization on the Performance of Bulk Heterojunction Solar Cells," *Advanced Energy Materials* 4 (2014): 1300693.

120. N. Gasparini, M. Salvador, S. Strohm, et al., "Burn-in Free Nonfullerene-Based Organic Solar Cells," *Advanced Energy Materials* 7 (2017): 1700770.

121. L. Yao, N. Guijarro, F. Boudoire, et al., "Establishing Stability in Organic Semiconductor Photocathodes for Solar Hydrogen Production," *Journal of the American Chemical Society* 142 (2020): 7795–7802.

122. A. Krishna, M. A. Akhavan Kazemi, M. Sliwa, et al., "Defect Passivation via the Incorporation of Tetrapropylammonium Cation Leading to Stability Enhancement in Lead Halide Perovskite," *Advanced Functional Materials* 30 (2020): 1909737.

123. J.-H. Kim, S. Seo, J.-H. Lee, et al., "Efficient and Stable Perovskite-Based Photocathode for Photoelectrochemical Hydrogen Production," *Advanced Functional Materials* 31 (2021): 2008277.

124. Y. Shao, Z. Xiao, C. Bi, Y. Yuan, and J. Huang, "Origin and Elimination of Photocurrent Hysteresis by Fullerene Passivation in CH3NH3PbI3 Planar Heterojunction Solar Cells," *Nature Communications* 5 (2014): 5784.

125. Y. Deng, S. Xu, S. Chen, X. Xiao, J. Zhao, and J. Huang, "Defect Compensation in Formamidinium–Caesium Perovskites for Highly Efficient Solar Mini-Modules With Improved Photostability," *Nature Energy* 6 (2021): 633–641.

126. Z. Ni, H. Jiao, C. Fei, et al., "Evolution of Defects During the Degradation of Metal Halide Perovskite Solar Cells Under Reverse Bias and Illumination," *Nature Energy* 7 (2022): 65–73.

127. C. Bi, X. Zheng, B. Chen, H. Wei, and J. Huang, "Spontaneous Passivation of Hybrid Perovskite by Sodium Ions From Glass Substrates: Mysterious Enhancement of Device Efficiency Revealed," *ACS Energy Letters* 2 (2017): 1400–1406.

128. M. Abdi-Jalebi, Z. Andaji-Garmaroudi, A. J. Pearson, et al., "Potassium- and Rubidium-Passivated Alloyed Perovskite Films: Optoelectronic Properties and Moisture Stability," *ACS Energy Letters* 3 (2018): 2671–2678.

129. D. S. Lee, J. S. Yun, J. Kim, et al., "Passivation of Grain Boundaries by Phenethylammonium in Formamidinium-Methylammonium Lead Halide Perovskite Solar Cells," *ACS Energy Letters* 3 (2018): 647–654.

130. J. S. Yun, J. Seidel, J. Kim, et al., "Critical Role of Grain Boundaries for Ion Migration in Formamidinium and Methylammonium Lead Halide Perovskite Solar Cells," *Advanced Energy Materials* 6 (2016): 1600330.

131. Z. Wang, Q. Lin, F. P. Chmiel, N. Sakai, L. M. Herz, and H. J. Snaith, "Efficient Ambient-Air-Stable Solar Cells With 2D–3D Heterostructured Butylammonium-Caesium-Formamidinium Lead Halide Perovskites," *Nature Energy* 2 (2017): 17135.

132. A. A. Sutanto, P. Caprioglio, N. Drigo, et al., "2D/3D Perovskite Engineering Eliminates Interfacial Recombination Losses in Hybrid Perovskite Solar Cells," *Chemistry* 7 (2021): 1903–1916.

133. X. Liu, T. Webb, L. Dai, et al., "Influence of Halide Choice on Formation of Low-Dimensional Perovskite Interlayer in Efficient Perovskite Solar Cells," *Energy & Environmental Materials* 5 (2022): 670–682.

134. D. L. McGott, C. P. Muzzillo, C. L. Perkins, et al., "3D/2D Passivation as a Secret to Success for Polycrystalline Thin-Film Solar Cells," *Joule* 5 (2021): 1057–1073.

27662098, 2026, 1, Downloaded from https://onlinelibrary.wiley.com/doi/10.1002/EXP.20240020 by CochraneChina, Wiley Online Library on [08/06/2026]. See the Terms and Conditions (https://onlinelibrary.wiley.com/terms-and-conditions) on Wiley Online Library for rules of use; OA articles are governed by the applicable Creative Commons License

135. D. B. Mitzi, "Templating and Structural Engineering in Organic–Inorganic Perovskites," *Journal of the Chemical Society, Dalton Transactions* 2001 (2001): 1–12.

136. G. Grancini and M. K. Nazeeruddin, "Dimensional Tailoring of Hybrid Perovskites for Photovoltaics," *Nature Reviews Materials* 4 (2019): 4–22.

137. D. B. Mitzi, C. A. Feild, W. T. A. Harrison, and A. M. Guloy, "Conducting Tin Halides With a Layered Organic-Based Perovskite Structure," *Nature* 369 (1994): 467–469.

138. Z. Wang, Q. Lin, F. P. Chmiel, N. Sakai, L. M. Herz, and H. J. Snaith, "Efficient Ambient-Air-Stable Solar Cells With 2D–3D Heterostructured Butylammonium-Caesium-Formamidinium Lead Halide Perovskites," *Nature Energy* 2 (2017): 17135.

139. G. Grancini, C. Roldán-Carmona, I. Zimmermann, et al., "One-Year Stable Perovskite Solar Cells by 2D/3D Interface Engineering," *Nature Communications* 8 (2017): 15684.

140. Y. Lin, Y. Bai, Y. Fang, et al., "Enhanced Thermal Stability in Perovskite Solar Cells by Assembling 2D/3D Stacking Structures," *Journal of Physical Chemistry Letters* 9 (2018): 654–658.

141. Y. Hu, J. Schlipf, M. Wussler, et al., "Hybrid Perovskite/Perovskite Heterojunction Solar Cells," *ACS Nano* 10 (2016): 5999–6007.

142. J. Xu, J. Cui, S. Yang, et al., "Stable High-Efficiency $CsPbI_2$ Br Solar Cells by Designed Passivation Using Multifunctional 2D Perovskite," *Advanced Functional Materials* 32 (2022): 2202829.

143. Y. Cho, A. M. Soufiani, J. S. Yun, et al., "Mixed 3D–2D Passivation Treatment for Mixed-Cation Lead Mixed-Halide Perovskite Solar Cells for Higher Efficiency and Better Stability," *Advanced Energy Materials* 8 (2018): 1703392.

144. J. Y. Ye, J. Tong, J. Hu, et al., "Enhancing Charge Transport of 2D Perovskite Passivation Agent for Wide-Bandgap Perovskite Solar Cells Beyond 21%," *Solar RRL* 4 (2020): 2000082.

145. C. Zhang, S. Wu, L. Tao, et al., "Fabrication Strategy for Efficient 2D/3D Perovskite Solar Cells Enabled by Diffusion Passivation and Strain Compensation," *Advanced Energy Materials* 10 (2020): 2002004.

146. T. Sekimoto, T. Matsui, T. Nishihara, R. Uchida, T. Sekiguchi, and T. Negami, "Influence of a Hole-Transport Layer on Light-Induced Degradation of Mixed Organic–Inorganic Halide Perovskite Solar Cells," *ACS Applied Energy Materials Journal* 2 (2019): 5039–5049.

147. K.-C. Hsiao, B.-T. Lee, M.-H. Jao, et al., "Chloride Gradient Render Carrier Extraction of Hole Transport Layer for High V and Efficient Inverted Organometal Halide Perovskite Solar Cell," *Chemical Engineering Journal* 409 (2021): 128100.

148. K. Ding, Y. Li, and S. R. Forrest, "Characterizing and Improving the Thermal Stability of Organic Photovoltaics Based on Halogen-Rich Non-Fullerene Acceptors," *ACS Applied Materials & Interfaces* 14 (2022): 5692–5698.

149. A. N. Cho and N. G. Park, "Impact of Interfacial Layers in Perovskite Solar Cells," *Chemsuschem* 10 (2017): 3687–3704.

150. Y. Bai, X. Meng, and S. Yang, "Interface Engineering for Highly Efficient and Stable Planar P-I-N Perovskite Solar Cells," *Advanced Energy Materials* 8 (2018): 1701883.

151. D. H. Kim, F. T. A. Wibowo, D. Lee, et al., "Non-Fullerene-Based Inverted Organic Photovoltaic Device With Long-Term Stability," *Energy & Environmental Materials* 6 (2023): e12381.

152. D. Yang, R. Yang, C. Zhang, et al., "Highest-Efficiency Flexible Perovskite Solar Module by Interface Engineering for Efficient Charge-Transfer," *Advanced Materials* 35 (2023): 2302484.

153. J. Zhang, J. Yang, R. Dai, et al., "Elimination of Interfacial Lattice Mismatch and Detrimental Reaction by Self-Assembled Layer Dual-Passivation for Efficient and Stable Inverted Perovskite Solar Cells," *Advanced Energy Materials* 12 (2022): 2103674.

154. W. Nie, H. Tsai, R. Asadpour, et al., "High-Efficiency Solution-Processed Perovskite Solar Cells With Millimeter-Scale Grains," *Science* 347 (2015): 522–525.

155. Q. Han, S.-H. Bae, P. Sun, et al., "Single Crystal Formamidinium Lead Iodide ($FAPbI_3$): Insight Into the Structural, Optical, and Electrical Properties," *Advanced Materials* 28 (2016): 2253–2258.

156. H. Tsai, R. Asadpour, J.-C. Blancon, et al., "Light-Induced Lattice Expansion Leads to High-Efficiency Perovskite Solar Cells," *Science* 360 (2018): 67–70.

157. Q. Jiang, L. Zhang, H. Wang, et al., "Enhanced Electron Extraction Using SnO_2 for High-Efficiency Planar-Structure $HC(NH_2)_2PbI_3$-Based Perovskite Solar Cells," *Nature Energy* 2 (2016): 16177.

158. Z. Hu, Z. Liu, L. K. Ono, et al., "The Impact of Atmosphere on Energetics of Lead Halide Perovskites," *Advanced Energy Materials* 10 (2020): 2000908.

159. X. Liu, Y. Cheng, B. Tang, et al., "Shallow Defects Levels and Extract Detrapped Charges to Stabilize Highly Efficient and Hysteresis-free Perovskite Photovoltaic Devices," *Nano Energy* 71 (2020): 104556.

160. Y. Wang, D. Zheng, K. Wang, et al., "Lattice Mismatch at the Heterojunction of Perovskite Solar Cells," *Angewandte Chemie International Edition* 63, no. 29 (2024): e202405878.

161. X. Guo, X. Huang, J. Su, et al., "Reducing the Interfacial Energy Loss via Oxide/Perovskite Heterojunction Engineering for High Efficient and Stable Perovskite Solar Cells," *Chemical Engineering Journal* 417 (2021): 129184.

162. V. J. Y. Lim, A. M. Ulatowski, C. Kamaraki, et al., "Air-Degradation Mechanisms in Mixed Lead-Tin Halide Perovskites for Solar Cells," *Advanced Energy Materials* 13 (2023): 2200847.

163. Y. Huang, J. Liang, Z. Zhang, et al., "Low-Temperature Phase-Transition for Compositional-Pure α-$FAPbI_3$ Solar Cells With Low Residual-Stress and High Crystal-Orientation," *Small Methods* 6 (2022): 2200933.

164. C. Wang, H. Yang, X. Xia, X. Wang, and F. Li, "Suppressing Interfacial Defect Formation Derived From In-Situ-Generated Polyethylenimine-Based 2D Perovskites to Boost the Efficiency and Stability NiO_x-Based Inverted Planar Perovskite Solar Cells," *Applied Surface Science* 548 (2021): 149276.

165. C. Wu, W. Fang, Q. Cheng, et al., "MXene-Regulated Perovskite Vertical Growth for High-Performance Solar Cells," *Angewandte Chemie* 134 (2022): e202210970.

166. G. Tang, P. You, Q. Tai, et al., "Solution-Phase Epitaxial Growth of Perovskite Films on 2D Material Flakes for High-Performance Solar Cells," *Advanced Materials* 31 (2019): 1807689.

167. Y. Xu, F. Liu, R. Li, et al., "Mxene Regulates the Stress of Perovskite and Improves Interface Contact for High-Efficiency Carbon-Based All-Inorganic Solar Cells," *Chemical Engineering Journal* 461 (2023): 141895.

168. Q. Zhou, J. Duan, J. Du, et al., "Tailored Lattice "Tape" to Confine Tensile Interface for 11.08%-Efficiency All-Inorganic $CsPbBr_3$ Perovskite Solar Cell With an Ultrahigh Voltage of 1.702 V," *Advancement of Science* 8 (2021): 2101418.

169. K. Anoop and T. Ahipa, "Recent Advancements in the Hole Transporting Layers of Perovskite Solar Cells," *Solar Energy* 263 (2023): 111937.

170. A. F. Akbulatov, L. A. Frolova, M. P. Griffin, et al., "Effect of Electron-Transport Material on Light-Induced Degradation of Inverted Planar Junction Perovskite Solar Cells," *Advanced Energy Materials* 7 (2017): 1700476.

171. Y. Yang, B. Xu, and J. Hou, "Reducing Depletion Region Width at Electrode Interface via a Hole-Transport Layer for Over 18% Efficiency in Organic Solar Cells," *Small* 20 (2024): 2306668.

172. M. Samir, E. Moustafa, O. Almora, et al., "CPE-Na-Based Hole Transport Layers for Improving the Stability in Nonfullerene Organic

27662098, 2026, 1, Downloaded from https://onlinelibrary.wiley.com/doi/10.1002/EXP.20240020 by CochraneChina, Wiley Online Library on [08/06/2026]. See the Terms and Conditions (https://onlinelibrary.wiley.com/terms-and-conditions) on Wiley Online Library for rules of use; OA articles are governed by the applicable Creative Commons License

Solar Cells: A Comprehensive Study," *ACS Applied Materials & Interfaces* 16 (2024): 16317–16327.

173. B. Rivkin, P. Fassl, Q. Sun, A. D. Taylor, Z. Chen, and Y. Vaynzof, "Effect of Ion Migration-Induced Electrode Degradation on the Operational Stability of Perovskite Solar Cells," *ACS Omega* 3 (2018): 10042–10047.

174. T. Bourgeteau, D. Tondelier, B. Geffroy, et al., "A H_2-Evolving Photocathode Based on Direct Sensitization of MoS_3 With an Organic Photovoltaic Cell," *Energy & Environmental Science* 6 (2013): 2706.

175. T. Bourgeteau, D. Tondelier, B. Geffroy, et al., "Enhancing the Performances of P3HT:PCBM–MoS_3-Based H_2-Evolving Photocathodes With Interfacial Layers," *ACS Applied Materials & Interfaces* 7 (2015): 16395–16403.

176. T. Bourgeteau, D. Tondelier, B. Geffroy, et al., "All Solution-Processed Organic Photocathodes With Increased Efficiency and Stability via the Tuning of the Hole-Extracting Layer," *Journal of Materials Chemistry A* 4 (2016): 4831–4839.

177. M. T. Hoang, N. D. Pham, J. H. Han, J. M. Gardner, and I. Oh, "Integrated Photoelectrolysis of Water Implemented on Organic Metal Halide Perovskite Photoelectrode," *ACS Applied Materials & Interfaces* 8 (2016): 11904–11909.

178. J. M. Yu, J. Lee, Y. S. Kim, et al., "High-Performance and Stable Photoelectrochemical Water Splitting Cell With Organic-Photoactive-Layer-Based Photoanode," *Nature Communications* 11 (2020): 5509.

179. R. Rhee, T. G. Kim, G. Y. Jang, et al., "Unassisted Overall Water Splitting With a Solar-to-Hydrogen Efficiency of Over 10% by Coupled Lead Halide Perovskite Photoelectrodes," *Carbon Energy* 5 (2023): e232.

180. T. H. Lee, S. A. J. Hillman, S. Gonzalez-Carrero, A. Difilippo, and J. R. Durrant, "Long-Lived Charges in Y6:PM6 Bulk-Heterojunction Photoanodes With a Polymer Overlayer Improve Photoelectrocatalytic Performance," *Advanced Energy Materials* 13 (2023): 2300400.

181. S. Nam, C. T. K. Mai, and I. Oh, "Ultrastable Photoelectrodes for Solar Water Splitting Based on Organic Metal Halide Perovskite Fabricated by Lift-Off Process," *ACS Applied Materials & Interfaces* 10 (2018): 14659–14664.

182. V. Andrei, R. L. Z. Hoye, M. Crespo-Quesada, et al., "Scalable Triple Cation Mixed Halide Perovskite–$BiVO_4$ Tandems for Bias-Free Water Splitting," *Advanced Energy Materials* 8 (2018): 1801403.

183. H. Choi, S. Seo, J.-H. Kim, et al., "An Organometal Halide Perovskite Photocathode Integrated With a MoS_2 Catalyst for Efficient and Stable Photoelectrochemical Water Splitting," *Journal of Materials Chemistry A* 9 (2021): 22291–22300.

184. H. Choi, Y. Y. Kim, S. Seo, et al., "Suppression of Undesired Losses in Organometal Halide Perovskite-Based Photoanodes for Efficient Photoelectrochemical Water Splitting," *Advanced Energy Materials* 13 (2023): 2300951.

185. C. Pornrungroj, V. Andrei, M. Rahaman, et al., "Bifunctional Perovskite-$BiVO_4$ Tandem Devices for Uninterrupted Solar and Electrocatalytic Water Splitting Cycles," *Advanced Functional Materials* 31 (2021): 2008182.

186. H. Choi, S. Seo, C. J. Yoon, et al., "Organometal Halide Perovskite-Based Photoelectrochemical Module Systems for Scalable Unassisted Solar Water Splitting," *Advancement of Science* 10 (2023): 2303106.

187. T. G. Kim, J. H. Lee, G. Hyun, et al., "Monolithic Lead Halide Perovskite Photoelectrochemical Cell With 9.16% Applied Bias Photon-to-Current Efficiency," *ACS Energy Letters* 7 (2022): 320–327.

188. I. Poli, U. Hintermair, M. Regue, et al., "Graphite-Protected $CsPbBr_3$ Perovskite Photoanodes Functionalised With Water Oxidation Catalyst for Oxygen Evolution in Water," *Nature Communications* 10 (2019): 2097.

189. Z. Zhu, M. Daboczi, M. Chen, Y. Xuan, X. Liu, and S. Eslava, "Ultrastable Halide Perovskite $CsPbBr_3$ Photoanodes Achieved With Electrocatalytic Glassy-Carbon and Boron-Doped Diamond Sheets," *Nature Communications* 15 (2024): 2791.

190. M. Daboczi, J. Cui, F. Temerov, and S. Eslava, "Scalable All-Inorganic Halide Perovskite Photoanodes With >100 h Operational Stability Containing Earth-Abundant Materials," *Advanced Materials* 35 (2023): 2304350.

191. H. Zhang, Y. Chen, H. Wang, et al., "Carbon Encapsulation of Organic–Inorganic Hybrid Perovskite Toward Efficient and Stable Photo-Electrochemical Carbon Dioxide Reduction," *Advanced Energy Materials* 10 (2020): 2002105.

192. N. Jiang, L. Zhang, Z. Li, et al., "Super-Hydrophilic Electrode Encapsulated Lead Halide-Perovskite Photoanode Toward Stable and Efficient Photoelectrochemical Water Splitting," *Chemical Engineering Journal* 492 (2024): 152024.

193. Y. Yang, S. Niu, D. Han, T. Liu, G. Wang, and Y. Li, "Progress in Developing Metal Oxide Nanomaterials for Photoelectrochemical Water Splitting," *Advanced Energy Materials* 7 (2017): 1700555.

194. Y. Sim, J. John, S. Surendran, B. Moon, and U. Sim, "Efficient Photoelectrochemical Water Splitting Reaction Using Electrodeposited Co_3Se_4 Catalyst," *Applied Sciences* 9 (2019): 16.

195. E. L. Miller, "Photoelectrochemical Water Splitting," *Energy & Environmental Science* 8 (2015): 2809–2810.

196. H. S. Han, W. Park, S. W. Hwang, et al., "(0 2 0)-Textured Tungsten Trioxide Nanostructure With Enhanced Photoelectrochemical Activity," *Journal of Catalysis* 389 (2020): 328–336.

197. H. S. Han, W. Park, A. Sivanantham, et al., "Facile Fabrication of Nanotubular Heterostructure for Enhanced Photoelectrochemical Performance," *Ceramics International* 47 (2021): 3972–3977.

198. S. Khamgaonkar, Q. Chen, K. Musselman, and V. Maheshwari, "Stable Perovskite Photocathodes for Efficient Hydrogen Evolution in Acidic and Basic Conditions," *Journal of Materials Chemistry A* 11 (2023): 20079–20088.

199. G. M. Carroll and D. R. Gamelin, "Kinetic Analysis of Photoelectrochemical Water Oxidation by Mesostructured Co-Pi/α-Fe_2O_3 Photoanodes," *Journal of Materials Chemistry A* 4 (2016): 2986–2994.

200. D. K. Lee, D. Lee, M. A. Lumley, and K.-S. Choi, "Progress on Ternary Oxide-Based Photoanodes for Use in Photoelectrochemical Cells for Solar Water Splitting," *Chemical Society Reviews* 48 (2019): 2126–2157.

201. K. Zhang and R. Zou, "Advanced Transition Metal-Based OER Electrocatalysts: Current Status, Opportunities, and Challenges," *Small* 17 (2021): 2100129.

202. J. H. Cho, J. Ma, and S. Y. Kim, "Toward High-Efficiency Photovoltaics-Assisted Electrochemical and Photoelectrochemical CO_2 Reduction: Strategy and Challenge," *Exploration* 3 (2023): 20230001.

203. W. Zhang, Z. Jin, and Z. Chen, "Rational-Designed Principles for Electrochemical and Photoelectrochemical Upgrading of CO_2 to Value-Added Chemicals," *Advancement of Science* 9 (2022): 2105204.

204. J. Chen, J. Yin, X. Zheng, et al., "Compositionally Screened Eutectic Catalytic Coatings on Halide Perovskite Photocathodes for Photoassisted Selective CO_2 Reduction," *ACS Energy Letters* 4 (2019): 1279–1286.

205. V. Andrei, B. Reuillard, and E. Reisner, "Bias-Free Solar Syngas Production by Integrating a Molecular Cobalt Catalyst With Perovskite–$BiVO_4$ Tandems," *Nature Materials* 19 (2020): 189–194.

206. Y. Xu, X. Liu, N. Cao, X. Xu, and L. Bi, "Defect Engineering for Electrocatalytic Nitrogen Reduction Reaction at Ambient Conditions," *Sustainable Materials and Technologies* 27 (2021): e00229.

207. W. Peng, Y. Feng, X. Yan, F. Hou, L. Wang, and J. Liang, "Multiatom Catalysts for Energy-Related Electrocatalysis," *Advanced Sustainable Systems* 5 (2021): 2000213.

208. C. Guo, J. Ran, A. Vasileff, and S.-Z. Qiao, "Rational Design of Electrocatalysts and Photo(Electro)Catalysts for Nitrogen Reduction to Ammonia (NH_3) Under Ambient Conditions," *Energy & Environmental Science* 11 (2018): 45–56.

27662098, 2026, 1, Downloaded from https://onlinelibrary.wiley.com/doi/10.1002/EXP.20240020 by CochraneChina, Wiley Online Library on [08/06/2026]. See the Terms and Conditions (https://onlinelibrary.wiley.com/terms-and-conditions) on Wiley Online Library for rules of use; OA articles are governed by the applicable Creative Commons License

209. G. Schrauzer and T. Guth, "Photolysis of Water and Photoreduction of Nitrogen on Titanium Dioxide," *Journal of the American Chemical Society* 99 (2002): 7189–7193.

210. G. Zhang, Y. Li, C. He, X. Ren, P. Zhang, and H. Mi, "Recent Progress in 2D Catalysts for Photocatalytic and Electrocatalytic Artificial Nitrogen Reduction to Ammonia," *Advanced Energy Materials* 11 (2021): 2003294.

211. S. Giddey, S. Badwal, C. Munnings, and M. Dolan, "Ammonia as a Renewable Energy Transportation Media," *ACS Sustainable Chemistry & Engineering* 5 (2017): 10231–10239.

212. W. Ye, M. Arif, X. Fang, M. A. Mushtaq, X. Chen, and D. Yan, "Efficient Photoelectrochemical Route for the Ambient Reduction of N_2 to NH_3 Based on Nanojunctions Assembled From MoS_2 Nanosheets and TiO_2," *ACS Applied Materials & Interfaces* 11 (2019): 28809–28817.

213. D. Liu, J. Wang, S. Bian, et al., "Photoelectrochemical Synthesis of Ammonia With Black Phosphorus," *Advanced Functional Materials* 30 (2020): 2002731.

214. K. Peramaiah, V. Ramalingam, H. C. Fu, et al., "Optically and Electrocatalytically Decoupled Si Photocathodes With a Porous Carbon Nitride Catalyst for Nitrogen Reduction With over 61.8% Faradaic Efficiency," *Advanced Materials* 33 (2021): 2100812.

215. G. Janani, S. Surendran, H. Choi, and U. Sim, "Photoelectrochemical Nitrogen Reduction Reaction," in*Photo- and Electro-Catalytic Processes* (Wiley, 2022), 339–387.

216. H. E. Kim, J. Kim, E. C. Ra, H. Zhang, Y. J. Jang, and J. S. Lee, "Photoelectrochemical Nitrate Reduction to Ammonia on Ordered Silicon Nanowire Array Photocathodes," *Angewandte Chemie* 134 (2022): e202204117.

217. F. Wang, Q. Ding, J. Ding, Y. Bai, H. Bai, and W. Fan, "Frustrated Lewis Pairs Boosting Photoelectrochemical Nitrate Reduction Over $ZnIn_2S_4/BiVO_4$ Heterostructure," *Chemical Engineering Journal* 450 (2022): 138260.

218. A. Tayyebi, R. Mehrotra, M. A. Mubarok, et al., "Bias-free Solar NH_3 Production by Perovskite-Based Photocathode Coupled to Valorization of Glycerol," *Nature Catalysis* 7 (2024): 510–521.

219. J. H. Kim, S. Han, Y. H. Jo, Y. Bak, and J. S. Lee, "A Precious Metal-Free Solar Water Splitting Cell With a Bifunctional Cobalt Phosphide Electrocatalyst and Doubly Promoted Bismuth Vanadate Photoanode," *Journal of Materials Chemistry A* 6 (2018): 1266–1274.

220. J. H. Kim, J.-W. Jang, Y. H. Jo, et al., "Hetero-Type Dual Photoanodes for Unbiased Solar Water Splitting With Extended Light Harvesting," *Nature Communications* 7 (2016): 13380.

221. J. H. Kim, D. Hansora, P. Sharma, J.-W. Jang, and J. S. Lee, "Toward Practical Solar Hydrogen Production—An Artificial Photosynthetic Leaf-to-Farm Challenge," *Chemical Society Reviews* 48 (2019): 1908–1971.

222. K. Sivula and R. van de Krol, "Semiconducting Materials for Photoelectrochemical Energy Conversion," *Nature Reviews Materials* 1 (2016): 15010.

223. A. M. K. Fehr, A. Agrawal, F. Mandani, et al., "Integrated Halide Perovskite Photoelectrochemical Cells With Solar-Driven Water-Splitting Efficiency of 20.8%," *Nature Communications* 14 (2023): 3797.

224. K. Maeda and K. Domen, "Photocatalytic Water Splitting: Recent Progress and Future Challenges," *Journal of Physical Chemistry Letters* 1 (2010): 2655–2661.

225. D. Hansora, J. W. Yoo, R. Mehrotra, et al., "All-Perovskite-Based Unassisted Photoelectrochemical Water Splitting System for Efficient, Stable and Scalable Solar Hydrogen Production," *Nature Energy* 9 (2024): 272–284.

27662098, 2026, 1, Downloaded from https://onlinelibrary.wiley.com/doi/10.1002/EXP.20240020 by CochraneChina, Wiley Online Library on [08/06/2026]. See the Terms and Conditions (https://onlinelibrary.wiley.com/terms-and-conditions) on Wiley Online Library for rules of use; OA articles are governed by the applicable Creative Commons License